Experimental Cell Research 395 (2020) 112179

Contents lists available at ScienceDirect

Experimental Cell Research

journal homepage: www.elsevier.com/locate/yexcr

Proteomic resolution of IGFN1 complexes reveals a functional interaction with the actin nucleating protein COBL

Tobias Cracknell [a], Steinar Mannsverk [b], Angus Nichols [a], Adam Dowle [c], Gonzalo Blanco [a,*]

[a] Department of Biology, University of York, York, YO32 5UQ, UK
[b] Department of Medical Biochemistry and Microbiology, Uppsala University, Uppsala, Sweden
[c] Technology Facility, Department of Biology, University of York, York, YO32 5UQ, UK

ARTICLE INFO

Keywords:
Myoblast
Z-disc
Cytoskeleton remodelling
Actin

ABSTRACT

The *Igfn1* gene produces multiple proteins by alternative splicing predominantly expressed in skeletal muscle. *Igfn1* deficient clones derived from C2C12 myoblasts show reduced fusion index and morphological differences compared to control myotubes. Here, we first show that G:F actin ratios are significantly higher in differentiating IGFN1-deficient C2C12 myoblasts, suggesting that fusion and differentiation defects are underpinned by deficient actin remodelling. We obtained pull-downs from skeletal muscle with IGFN1 fragments and applied a proteomics approach. The proteomic composition of IGFN1 complexes identified the cytoskeleton and an association with the proteasome as the main networks. The actin nucleating protein COBL was selected for further validation. COBL is expressed in C2C12 myoblasts from the first stages of myoblast fusion but not in proliferating cells. COBL is also expressed in adult muscle and, as IGFN1, localizes to the Z-disc. We show that IGFN1 interacts, stabilizes and colocalizes with COBL and prevents the ability of COBL to form actin ruffles in COS7 cells. COBL loss of function C2C12-derived clones are able to fuse, therefore indicating that COBL or the IGFN1/COBL interaction are not essential for myoblast fusion.

1. Introduction

IGFN1 (Immunoglobulin-Like And Fibronectin Type III Domain Containing 1) was first identified as a protein fragment in a Yeast-two-hybrid assay using the KY protein as bait [1]. Subsequently, both proteins were localized at the Z-disc [2]. Mutations in the *ky* gene cause muscle disease in mice and humans [3–6], indicating a crucial role for the corresponding protein in skeletal muscle. KY has recently been implicated in protein turnover [7], in agreement with previous reports showing accumulation of the actin binding crosslinkers filamin C and Xin in muscles from *ky/ky* mice [1,8]. However, mechanistic roles have not been established for KY or IGFN1, hence we do not yet understand the role that these proteins play in the maintenance of skeletal muscle. The *Igfn1* gene produces multiple proteins by alternative splicing, predominantly in skeletal muscle and heart [2]. Full-length IGFN1 contains a series of 11 fibronectin and immunoglobulin-like domains distributed in three N- and eight C-terminal domains separated by a large disordered segment. The latter is alternatively spliced in the smaller IGFN1_v1 isoform [2]. The domain composition of IGFN1 is reminiscent of other sarcomeric proteins that bear an inherent flexible structure that allows them to maintain protein interactions through cycles of contraction and relaxation (e.g. Ref. [9]) whilst anchored to the cytoskeleton (see Ref. [10] for a review). Disruptive mutations in *Igfn1* were recently generated by CRISPR/Cas9 mutagenesis in C2C12 myoblasts [11]. *Igfn1* deficient clones showed reduced fusion index and gross morphological differences to C2C12 myotubes, indicating a role for IGFN1 in myoblast fusion and differentiation [11]. To gain an insight into the possible mechanisms played by IGFN1, we measured G:F actin ratios and ressoved IGFN1 protein complexes by proteomics. These results highlighted cytoskeletal remodelling as a plausible role for IGFN1. Therefore an interaction with the actin nucleating protein COBL was selected for further analysis.

2. Results

2.1. Reduced actin remodelling in IGFN1-deficient C2C12 myoblasts

The domain composition of IGFN1 resembles that of other cytoskeletal associated proteins, which led us to hypothesize that it may play a scaffolding role to promote fusion by facilitating local actin remodelling. To test this, we looked at the ratio of globular actin (G) and

* Corresponding author.
E-mail address: gonzalo.blanco@york.ac.uk (G. Blanco).

https://doi.org/10.1016/j.yexcr.2020.112179
Received 4 May 2020; Received in revised form 6 July 2020; Accepted 11 July 2020
Available online 5 August 2020

Abbreviations

IGFN1	Immunoglobulin-Like And Fibronectin Type III Domain Containing 1
KO19	a C2C12 derived cell line with disruptive mutations on both alleles of *Igfn1* exon 13
COBL:	Protein cordon-bleu
KY	Kyphoscoliosis peptidase
EDL/TA	Extensor digitorum longus/tibialis anterior muscles
GM	Growth medium
DM	Differentiation medium
qPCR	Quantitative polymerase chain reaction
IPTG	Isopropyl β-D-1-thiogalactopyranoside
LDS	Lithium dodecyl sulfate

filamentous actin (F) in control cells (C2C12), IGFN1 deficient (KO19) and a rescued cell line (KO19+IGFN1_v1, which derives from KO19 stably transfected with IGFN1_v1:tdTomato) (Fig. 1). Following the protocol as described in Methods, F-actin was consistently purified from all cell lines maintained for 7 days in differentiation medium and therefore we selected this time point for the analysis. Early time points did not produce sufficient yields of F-actin for comparisons (data not shown). Quantifications from 8 independently generated replicas showed a significant G:F actin ratio increase in KO19 cells (Fig. 1B). A trend towards rescuing this defect was observed in the KO19+IGFN1_v1 cell line ($p = 0.056$, Fig. 1A and B). All cell lines showed similar levels of expression of total actin relative to GAPDH (Fig. 1C), indicating that higher G:F actin ratios in the KO19 cells were not caused by lower actin expression levels but from lower polymerization activity. It would thus appear that IGFN1 contributes to the actin polymerization activity in C2C12 cells. Given that IGFN1 lacks any enzymatic domain, we next applied a proteomics approach in an attempt to identify partners that could mediate actin polymerization activity.

2.2. Proteomic resolution of IGFN1 complexes

To facilitate expression in *E. coli*, smaller fragments of IGFN1 containing the first three globular domains (pET161-DEST-Igfn1 (d1-d3)) or the last six globular domains (pET161-DEST-Igfn1 (d6-d11)) (Fig. 2A) were cloned in frame with a polyhistidine tag. Expression was optimised to produce sufficient yields of protein bound to Ni-NTA beads (Fig. 2B). Comparable amounts of purified proteins were used in the following pull-down assays. Mouse skeletal muscle extracts were used to isolate protein complexes for IGFN1(d1-d3), IGFN11(d6-d11) and LacZ as negative control from three biological replicas. Protein complexes were resolved on protein gels and the lanes cut and processed for LC-MS/MS analysis as described in Methods. Lists of proteins identified for each bait

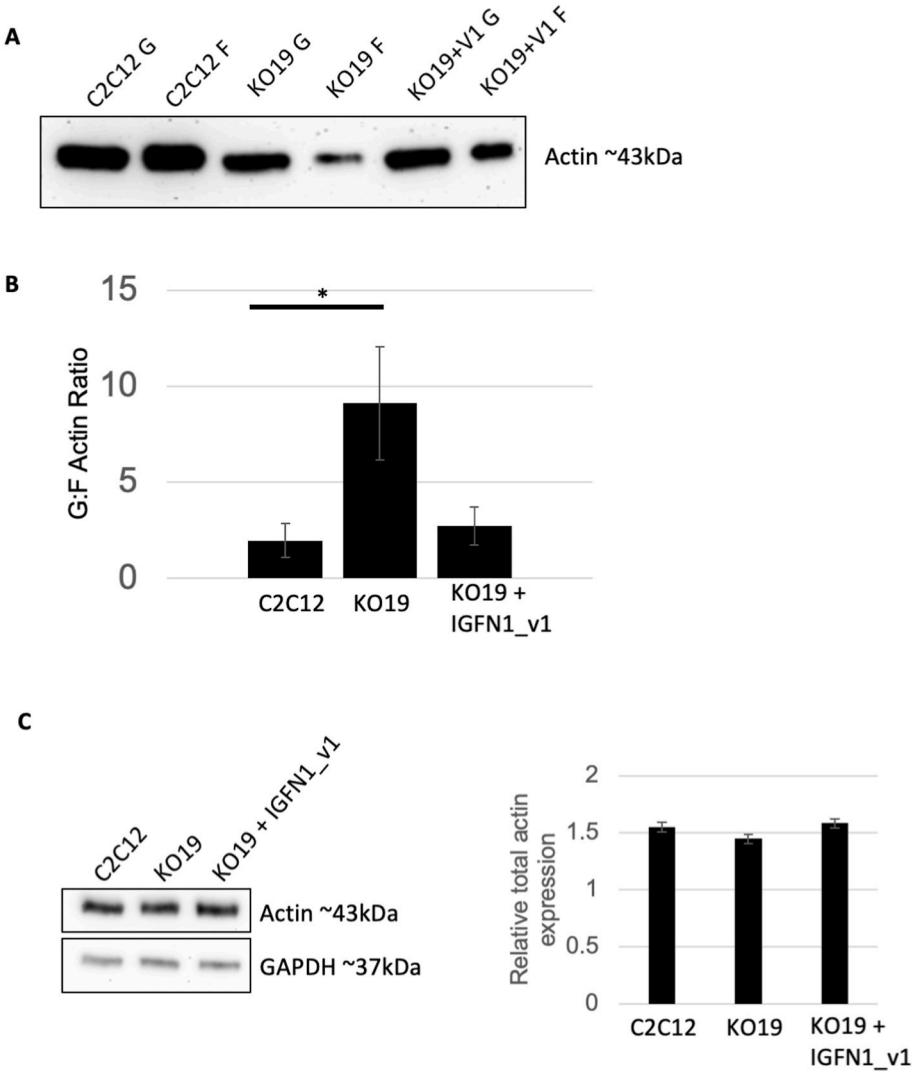

Fig. 1. Differentiating IGFN1 knockout myoblasts have a higher G:F actin ratio. A) Representative Western blot (n = 8) against actin using 7 day differentiated cells. Protein extracts from C2C12, IGFN1 knockout (KO19) and KO19 stably transfected with IGFN1_v1 (KO19+IGFN1_v1) cell lines were processed to obtain globular (G) or filamentous (F) actin fractions and loaded as indicated. B) G:F actin ratio of C2C12, KO19 and KO19+IGFN1_v1, as labelled. One-way ANOVA showed a significant effect of cell type at the $p < 0.05$ level [$F(2, 22) = 4.665$, $p = 0.02$]. Post-hoc comparisons using the Tukey HSD test revealed a significant difference between the mean G:F ratio of C2C12 and KO19 cells ($p < 0.05$). C) Representative Western blot (n = 5) of total actin from C2C12, KO19 and KO19+IGFN1_v1. Quantifications of n = 5 blots shown on the histogram. Note that all cell lines show similar levels of total actin.

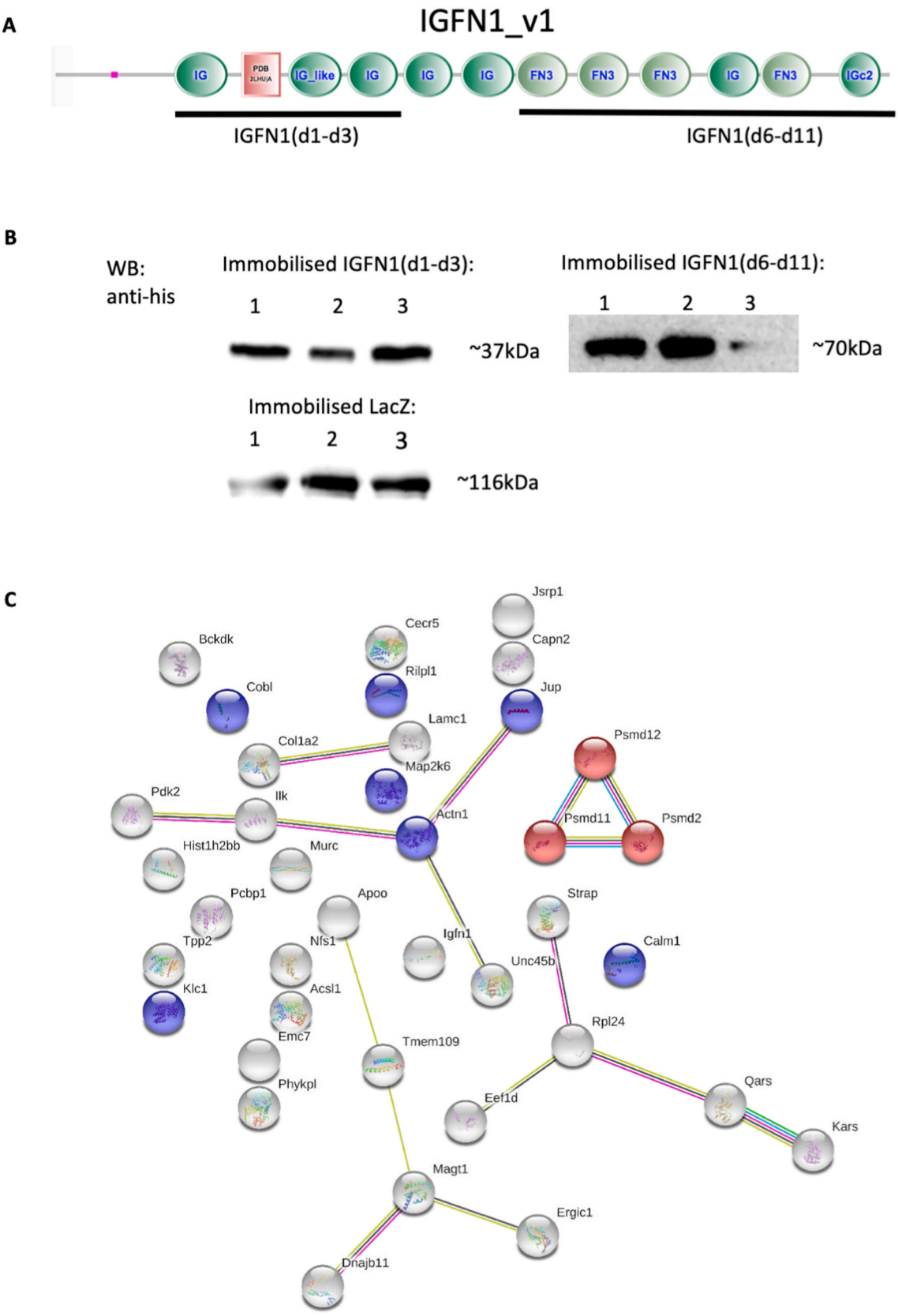

Fig. 2. Proteomics results. A) SMART (http://smart.embl-heidelberg.de) predicted domain composition of mouse IGFN1_v1 (UniProtKBreference protein sequence Q3KNY0-04) with the globular domains spanning the two fragments used as baits for pull-downs (IGFN1(d1-d3) and IGFN1(d6-d11)) indicated by the black lines. B) Western blots from immobilized his-tagged recombinant proteins detected with anti-his antibodies. C) STRING-Db output of the putative IGFN1 interactome obtained from all unique hits present in supp Table 1. Lines between nodes represent interactions found in the STRING database, the number of interactions is higher than would be expected from a random set of proteins (PPI enrichment p-value = 0.00983). Functional enrichments in the cytoskeleton and the proteasome are highlighted in blue and red, respectively (FDR = 0.033 and 0.0038 respectively).

were filtered to require a minimum of two unique identified peptides. Probabilities were assigned by the Protein Prophet algorithm [12] and the following criteria was applied to determine presence or absence in each pull-down: 1) Inclusion required protein identification probability of greater than 95% in at least two of three biological replicates; 2) Exclusion required protein identification probability of less than 95% in all three biological replicas. The filtered data set indicating proteins identified with fragment Igfn1 (d1-d3), Igfn1 (d6-d11) or both is presented in Supplementary Table 1 (full tables specifying results for each biological replica for peptide and protein identifications are provided in supplementary material as Supplementary Table 2 and Table 3, respectively). A small number of proteins, including COBL, were identified as common in both pull-downs. We did not interpret this as a sign of non-specificity since previous assays in the yeast-two-hybrid with N- and C-term IGFN1 fragments also showed that filaminC was able to interact with both fragments [2]. The full list contains other previously identified binding partners including filaminC, titin, PDLIM3, ACTIN and EEF1A [2,13]. Specificity was further supported by the identification of α-actinin and IGFN1 itself, which is consistent with previously documented interactions of IGFN1 with other Z-disc proteins [1,2]. The list of accepted interacting proteins was submitted to the STRING database [14] to obtain a graphical illustration of functional networks (Fig. 2C). The STRING output using default settings shows the cytoskeleton and the proteasome as the main networks. Since IGFN1 deficient C2C12 derived myoblasts show fusion defects [11] and myoblast fusion relies on actin remodelling (see Discussion), we selected the interaction with the actin nucleating protein COBL for further analysis.

2.3. *Cobl expression in adult skeletal muscle*

Cobl has not been previously studied in skeletal muscle. We identified *Cobl* cDNA by RT-PCR in a mouse cDNA skeletal muscle library and in primary cDNA from skeletal muscle. Full length *Cobl* was then cloned into a Gateway compatible entry vector and sequence verified. The sequence matched ENSEMBL mouse Cobl-201 variant, which predicts a protein of 1337 AA identical to UniProtKB Q5NBX1 (see Fig. 3A for the predicted genomic structure and annotated domain composition of COBL). No shorter alternative *Cobl* cDNAs were identified in skeletal muscle using primers from exon 1 to exon 14 (Fig. 3A), indicating that skeletal muscle expresses only full length COBL. We confirmed the expression of *Cobl* in skeletal muscle and differentiated C2C12 cells protein extracts by Western Blots and immunofluorescence. Polyclonal anti-COBL antibodies produced a band higher than the predicted 144 kDa (Fig. 3B); the specificity of this band was ascertained in later experiments, (see Fig. 8B in "*Generation of a C2C12-derived COBL Knockout Cell Line*"). On longitudinal sections of skeletal muscle, these antibodies provided a signal to the Z-disc (Fig. 3C), consistent with the localization of IGFN1 to this sarcomeric band [2]. Strong non-specific signals were also obtained with these antibodies (Fig. 3C). To further ascertain COBL localization in the adult fibre, full length *Cobl* was transferred from the entry vector to a mammalian expression vector in frame with TdTomato (pDEST47-COBL-tdTomato). pDEST47-COBL-tdTomato was then electroporated into the TA/EDL muscles of 6–7 weeks old C3H/HeH mice and allowed to express for 10 days. Confocal images of longitudinal sections of sections from electroporated mice showed a striated signal for COBL-tdTomato that colocalized with the α-actinin antibody EA-53 (Fig. 3D), therefore confirming the Z-disc localization of COBL. Non-electroporated fibres and fibres electroporated with tdTomato alone showed no signal and diffuse signal, respectively.

2.4. *IGFN1 interacts with and modifies COBL activity in COS7 cells*

To test the IGFN1/COBL interaction in a heterologous system, COS7 cells were co-transfected with either pDEST47-IGFN1_v1-V5 and pDEST47-COBL-tdTomato or with pDEST47-LacZ-V5 and pDEST47-COBL-tdTomato. After 48 h of expression, cells were lysed and lysates incubated against either anti-V5 IgG agarose beads or IgG Agarose beads as additional control for non-specific bindings. The bead pellets were then interrogated on Western blots for the presence of recombinant V5 tagged proteins and COBL-tdTomato using anti-V5 and anti-Cobl antibodies, respectively. A band at the expected molecular weight of COBL-tdTomato was detected only in samples from COS7 cells transfected with pDEST47-IGFN1_v1-V5 and pDEST47-COBL-tdTomato (Fig. 4A). COBL-tdTomato was detected at negligible levels in the LacZ-V5 and beads only negative control lanes. The interaction between recombinant COBL and IGFN1_v1 detected in COS7 cells is likely to be direct as COBL is not expressed in this cell line (Fig. 4B).

Nucleo-cytoplasmic localizations of IGFN1-V1 have previously been reported in proliferative cells and electroporated adult muscles [2,11], whilst COBL has always been reported at the cytoplasm (e.g. Ref. [16]). We therefore asked whether ectopically expressed COBL in COS7 cells would have any effect on the subcellular localization of IGFN1. COS7 cells were transfected with either pDEST47-IGFN1_v1-GFP and pDEST47-COBL-tdTomato or pDEST47-IGFN1_v1-GFP and pDEST47-tdTomato. In COS7 cells transfected with a single construct, IGFN1_v1-GFP predominantly accumulated in the nucleus whilst COBL-tdTomato was expressed in the cytoplasm (Fig. 4C). In cells expressing both IGFN1_v1-GFP and COBL-tdTomato a much higher proportion of cells expressing IGFN1_v1-GFP in the cytoplasm was observed (Fig. 4D), suggesting that an interaction with COBL may prevent IGFN1_v1 from translocating to the nucleus. This nuclear to cytoplasmic expression shift for IGFN1_v1-GFP was not observed in cells co-transfected with IGFN1_v1-GFP and tdTomato (Fig. 4D).

To characterize co-localization in more detail, co-transfections of muscle cells and electroporations of adult muscle were carried out with pDEST47-IGFN1_v1-GFP and pDEST47-COBL-tdTomato, but repeated attempts failed to yield enough cells expressing both recombinant proteins, most likely because of their large molecular weights. We therefore applied confocal microscopy to COS7 cells in order to quantify the levels of colocalization for IGFN1 and COBL, as these cells appear to cope better with the simultaneous expressions of recombinant proteins each exceeding 200 kDa. Volocity software (www.perkinelmer.com) was used to quantify the Pearson's correlation coefficient, with the Costes method [15] used for setting thresholds. Pearson's correlation coefficient was significantly higher in cells co-transfected with IGFN1_v1-GFP and COBL-tdTomato than in cells co-transfected with IGFN1_v1-GFP and tdTomato constructs (Fig. 4E and F) indicating that IGFN1_v1 and COBL co-localize in a non-muscle cell.

2.5. *Cobl expression in C2C12 differentiation*

To test whether the putative IGFN1/COBL interaction could be implicated in the differentiation defects associated with IGFN1 deficiency in vitro [11] we first looked into the expression of *Cobl* at protein and transcript levels in C2C12 cells. Full length COBL protein was found to be weakly expressed in proliferating cells, but then robustly expressed in fully confluent C2C12 cells starting to differentiate (D0) and thereafter (D1, D7, Fig. 5A). A similar expression profile was found in the KO19 cell line, a C2C12 derived cell line with disruptive mutations on both alleles of *Igfn1* exon 13 [11]. However, COBL protein levels in differentiating C2C12 compared to KO19 myoblasts appear similar or higher (examples in Fig. 5A) while quantitative reverse transcriptase PCR showed that transcript levels of *Cobl* were significantly higher in the KO19 cell line (Fig. 5B). Higher *Cobl* transcript levels in the KO19 cell line did not correlate with higher COBL protein levels, thus suggesting that IGFN1 may contribute to stabilize COBL in control cells. To test this possibility further, we looked at the expression of COBL in transfected COS7 cells cotransfected with IGFN1_v1-GFP or GFP alone and exposed to cycloheximide. COBL expression levels appear higher in the presence of IGFN1 before and at every point of the cycloheximide treatment (Fig. 5C). Altogether, these results suggest IGFN1 contributes to COBL stabilization. We next tested whether the COBL/IGFN1 interaction

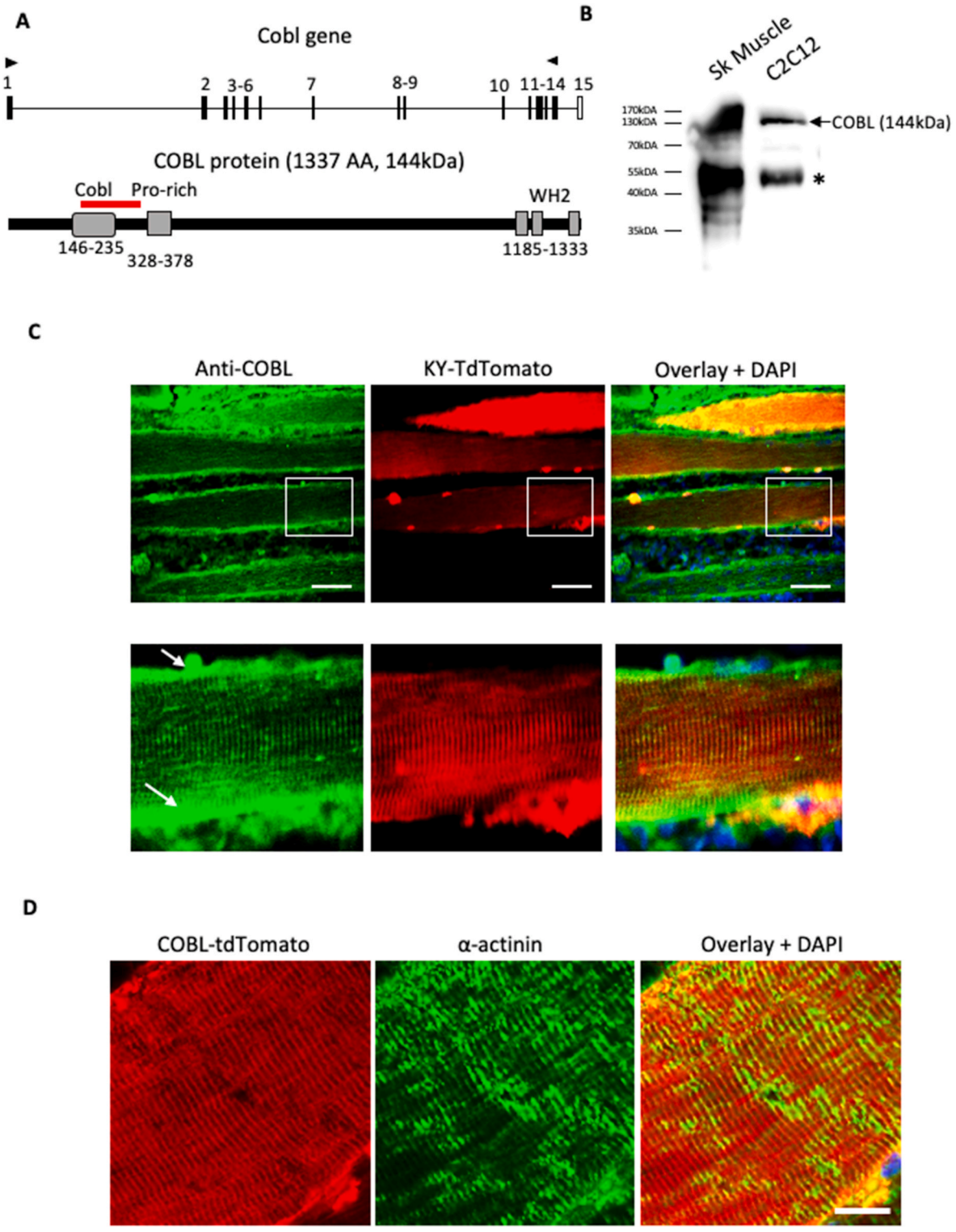

Fig. 3. COBL is a Z-disc associated protein in mouse skeletal muscle. A) Above, intron/exon structure of the mouse *Cobl* gene with exons numbered according to the predicted ENSEMBL Cobl-201 (ENSMUST00000046755.13). ENSEMBL Cobl-201 matches the sequence from the mouse cDNA amplified from a skeletal muscle library using the indicated primers (arrow tips). No shorter alternative COBL cDNAs were obtained. The mouse skeletal muscle cDNA predicts a protein of 1337 AA identical to UniProtKB Q5NBX1. Below, the mouse COBL protein with domains annotated as follows: Cobl, ubiquitin-like fold domain (IPR019025); Pro-rich, indicates a proline rich region (compositional bias); WH2, Wiskott-Aldrich homology 2 domain (IPR003124). The antigen used for anti-Cobl antibodies is indicated by the red bar. B) Western blot against COBL using a Gastrocnemius muscle and a 7-day differentiated C2C12 cell extracts confirms expression of COBL in mouse skeletal muscle tissue and in the C2C12 myoblast cell line. The asterisk indicates cross reactivity. C) Longitudinal cross-sections of mouse gastrocnemius muscle. Sections are from mice electroporated with a KY-TdTomato vector to identify the Z-disc (red) and incubated with anti-COBL antibody (green). Note that COBL antibodies identify a striated pattern that coincides with the z-disc as well as non-specific signals (white arrows). The insets (white squares) are shown magnified below. Scale bar is 50 μm. D) Sections from Tibialis Anterior muscle from mice electroporated with a COBL-Tdtomato recombinant cDNA (red) and incubated with EA-53 antibodies against alpha-actinin (green). Note that recombinant COBL-tdTomato also localizes to the Z-disc. Scale bar is 15 μm.

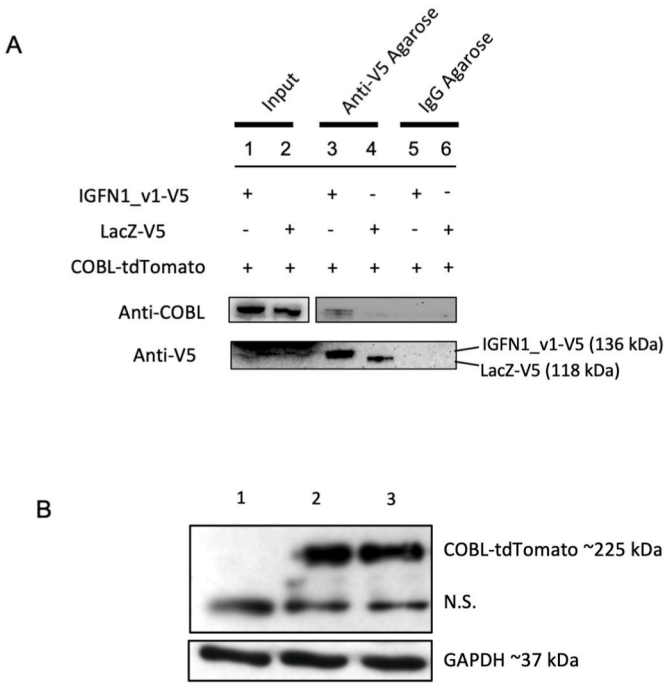

Fig. 4. IGFN1_v1 interacts with COBL and shifts from nuclear to cytoplasmic localization in the presence of COBL in COS7 cells. A) IGFN1_v1 and COBL coimmunoprecipitate in a pull-down interaction assay. Representative blots (n = 3) are shown from pulldowns of cell extracts from COS7 cells co-transfected with either pDEST47-IGFN1_v1-V5 and pDEST47-COBL-tdTomato or with pDEST47-V5 and pDEST47-COBL-tdTomato to control for non-specific binding between the two tags. Pull-downs were performed against either anti-V5 IgG agarose beads or IgG Agarose beads as a control for non-specific protein binding to the beads. Note that COBL-tdTomato is specifically pulled down together with IGFN1_v1-V5 only. B) Western blot of untransfected (1) and transfected COS7 cells with COBL-tdTomato (2 and 3) probed with anti-COBL antibodies and GAPDH as loading control. No endogenous expression of COBL is detected in COS cells. N.S. denotes cross reactivity. C) Representative images of COS7 cells co-transfected with either pDEST47-IGFN1_v1-GFP and pDEST47-COBL-tdTomato (top row) or with pDEST47-IGFN1_v1-GFP and pDEST47-tdTomato (bottom row). IGFN1_v1-GFP is generally found in the nucleus when expressed on its own or with tdTomato (white arrows). IGFN1_v1-GFP shows perinuclear and cytoplasmic expression when co-transfected with COBL-tdTomato. Scale bar represents 30 μm. D) Pie charts illustrating proportion of cells showing localization of IGFN1_v1-GFP as nuclear, cytoplasmic or both when co-transfected with either pDEST47-COBL-tdTomato or pDEST47-tdTomato. Note that after the cotransfection indicated on the left column, cells were classified as singly transfected ("IGFN1_v1-GFP only") or doubly transfected ("IGFN1_v1-GFP + COBL-tdTomato" or "IGFN1_v1-GFP + tdTomato") as indicated at the top of each pie chart. Note the shift in size of the red sector in cells cotransfected with IGFN1_v1-GFP and COBL-tdTomato, indicating a much higher proportion of IGFN1_v1-GFP cytoplasmic expression. The predominant blue sectors indicate that cells expressing IGFN1_v1-GFP alone or both IGFN1_v1-GFP and tdTomato show mainly nuclear localization. (n > 30 cells for each condition). E) IGFN1_v1-GFP colocalizes with COBL-tdTomato in COS7 cells. Representative images of COS7 cells co-transfected with either pDEST47-IGFN1_v1-GFP and pDEST47-COBL-tdTomato or with pDEST47-IGFN1_v1-GFP and pDEST47-tdTomato. The selected range of interest (ROI) for individual cells expressing both constructs and the corresponding images showing pixels where co-localization is apparent are shown. Scale bar represents 30 μm. F) Histogram showing mean Pearson's correlation coefficient values as quantification of colocalization. Volocity software (Quorum Technologies) was used for analysis with the Costes method [15] used to set thresholds. Colocalization was significantly higher in cells co-transfected with pDEST47-IGFN1_v1-GFP and pDEST47-COBL-tdTomato (IGFN1_v1 + COBL, n = 25) than cells transfected with pDEST47-IGFN1_v1-GFP and pDEST47-tdTomato (IGFN1_v1 + tdTomato, n = 12) (students t-test, $p < 0.01$).

resulted in an enhancement or inhibition of COBL specific activity.

2.6. IGFN1_v1 inhibits COBL-induced membrane ruffle formation

We selected COS7 cells for these experiments because COBL has been shown to induce ruffles formation in these cells [16]. Ruffles were detected by the accumulation of phalloidin positive structures at the membrane edge. Ruffles were readily detectable and quantifiable in cells transfected with COBL-tdtomato, which showed localization of COBL-tdTomato and phalloidin to the same structures (Fig. 6, see Methods for details). Ruffles were not detected in cells transfected with maxGFP, tdTomato or IGFN1_v1-GFP (Fig. 6). In addition, detail quantifications showed that cells cotransfected with COBL-tdtomato and IGFN1_v1-GFP did not show ruffles, while cells cotransfected with COBL-tdtomato and maxGFP showed similar levels of ruffles to cells transfected with COBL-tdtomato alone (Fig. 6B). Thus, IGFN1_v1 inhibits COBL-induced membrane ruffle formation in COS7 cells. Altogether, these results suggest that IGFN1 modulates COBL activity.

2.7. Overexpression of COBL increases myoblast fusion

To examine the effect of COBL overexpression on the differentiation of myotubes pDEST47-COBL-tdTomato and pDEST47-tdTomato transfected C2C12 cells were differentiated for 7 days. On day 7, cells were fixed and the number of nuclei within a cell expressing either COBL-tdTomato or tdTomato alone was counted. The fusion index of these cultures, expressed as the proportion of cells with 3 or more nuclei, could not be calculated because only a small proportion of cells expressed the transfect construct. However, we observed a sufficient number of myotubes expressing COBL-tdtomato or tdTomato to allow for comparative quantifications of the number of nuclei contained within the tubes. We observed that pDEST47-COBL-tdTomato expressing myotubes contained significantly more nuclei than pDEST47-tdTomato expressing myotubes, indicating that myoblasts overexpressing COBL are more likely to fuse than myoblasts expressing tdTomato (Fig. 7).

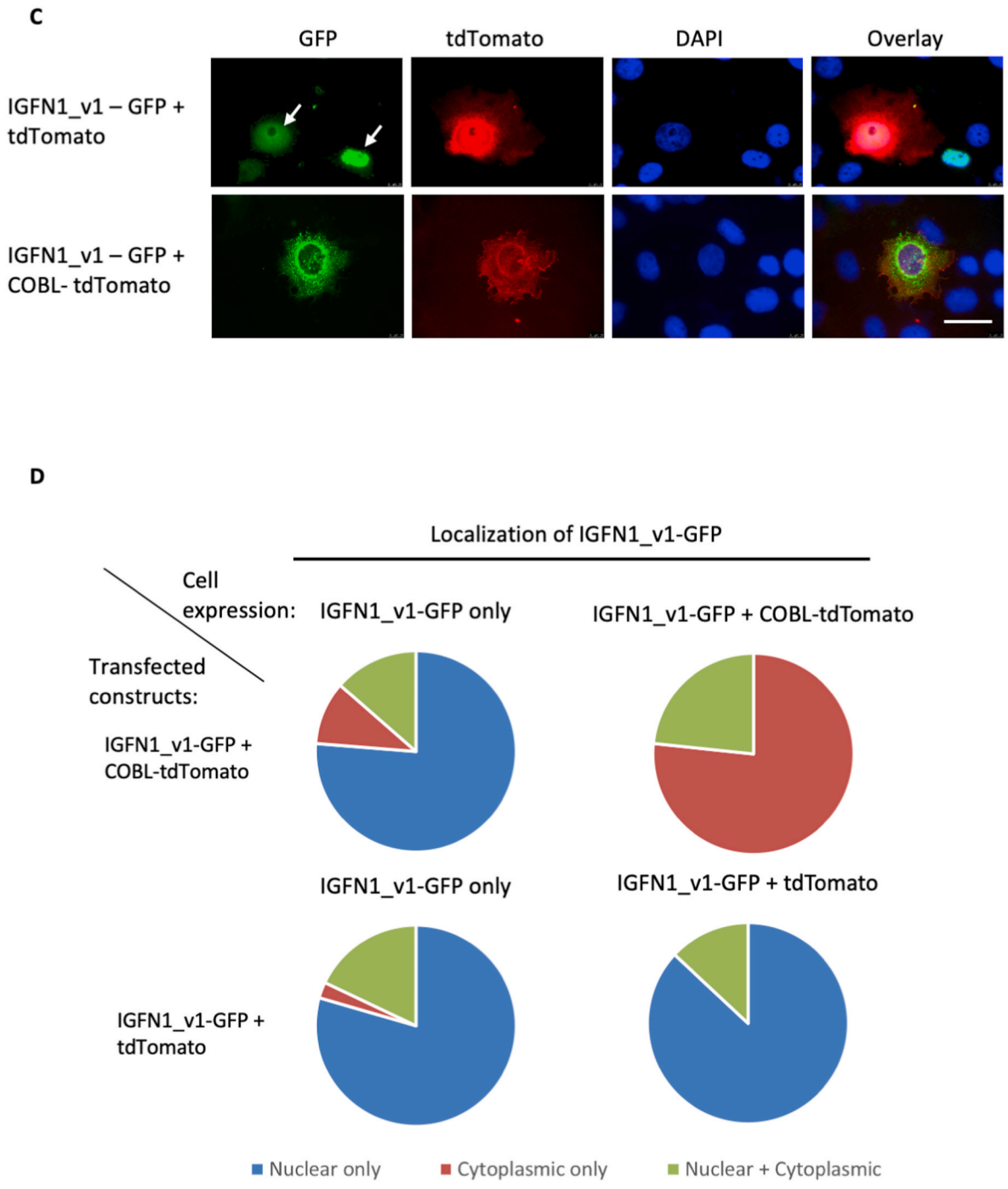

Fig. 4. (*continued*).

2.8. Generation of a C2C12-derived COBL Knockout Cell Line

To test whether the previously observed fusion defects in IGFN1-deficient myoblasts are mediated by COBL, *Cobl* knockout C2C12-derived clones were generated. Selection was applied *en masse* but also by individual clone selection. Selected clones were tested for amplification of exon 3 to confirm genetic disruption of the locus (Fig. 8A). Clones KO15, KO18 and KO23 failed to amplify exon 3 and showed total loss of COBL by Western blots (Fig. 8B). This analysis showed that the relevant band representing COBL in Western blots migrates at ~170 kDa, as this is the only band absent in the COBL knockout clones, thus confirming that full-length COBL does not migrate to its predicted molecular weight of ~144 kDa. Interestingly, cells selected *en masse* showed amplification of exon 3 and displayed similar levels of COBL expression to control cells (Fig. 8B). Further characterization was therefore carried out only on clones KO15, KO18 and KO23.

To examine fusion and differentiation, clones KO15, KO18 and KO23 were allowed to differentiate for 7 days, fixed and stained with EA53 antibodies against α-actinin. KO15 did not show any evidence of expression of α-actinin. Myotubes from clones 18 and 23 showed predominantly irregular high density patches of α-actinin and never achieved a striated pattern, indicating that these clones failed to form sarcomeres (see detailed images in Fig. 8C). In an attempt to enhance myotube differentiation, these clones were maintained in differentiation medium for up to 38 days with no observable change in the number of myotubes or their α-actinin pattern. As expected, C2C12 cells

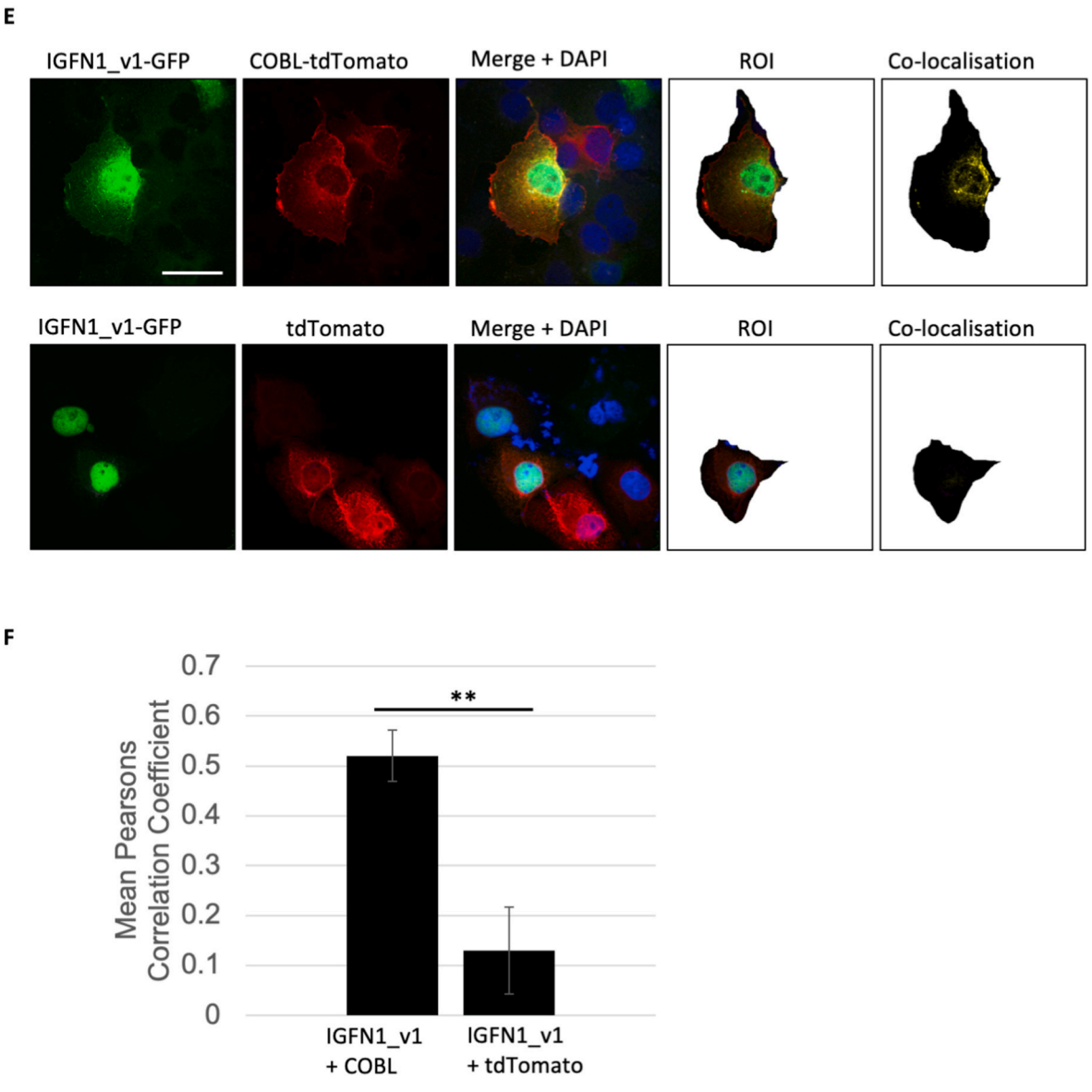

Fig. 4. (*continued*).

differentiated and showed α-actinin organized in a striated pattern within 7 days (Fig. 8C). Differentiation and fusion indexes expressed, respectively, as the fraction of nuclei within an α-actinin positive structure to the total number of nuclei in a given field and the fraction of α-actinin positive cells with three or more nuclei to the total number of cells expressing α-actinin, were very low for KO18 and KO23 compared to control cells (Fig. 8F). Since fusion could still be observed, we conclude that COBL is not necessary for fusion. The irregular α-actinin pattern in KO18 and KO23 suggests that COBL may facilitate full myofibrillogenesis in vitro. As attested by the different behaviour shown by KO15, aberrant differentiation shown by KO18 and KO23 could have been caused by the process of clonal selection itself rather than the absence of COBL. To assess this, pDEST47-COBL-tdTomato was re-introduced into KO18 and KO23. Transient transfections levels of these clones were not sufficient to evaluate differentiation parameters (data not shown). Therefore, cell lines stably expressing COBL-tdtomato were derived from KO18 and KO23. Stable expression of COBL-tdtomato was verified by fluorescence microscopy for clones T18B5 and T18A7 (derived from clone 18) and for T23G5 and T23B7 (derived from clone 23) (data not shown). These clones were allowed to differentiate as above. No significant differences were found in the fusion and differentiation indexes calculated for all these cell lines (Fig. 8F). Therefore, the reduced fusion and differentiation defects in KO18 and KO23 were not caused by COBL deficiency but were most likely a consequence of clonal selection and subsequent cell passages. We noted that reintroduction of COBL prevented the appearance of α-actinin random aggregates (compare KO18 and KO23 in Fig. 8C with example images of its derived clones Fig. 8D and E).

3. Discussion

Igfn1 deficient C2C12 derived cell lines show reduced fusion, impaired differentiation [11] and a significant increase of G:F actin ratio. We hypothesized that these phenotypes are mediated by other proteins scaffolded by IGFN1 at the appropriate place and time during differentiation, since IGFN1 lacks any enzymatic domain. To address this hypothesis, we used IGFN1 fragments as baits to pull-down complexes from adult skeletal muscle and applied a proteomics approach to resolve them. The specificity of the identified targets was supported by the identification of α-actinin and IGFN1 itself, as these are consistent with the Z-disc localization of IGFN1 and its previously documented interactions with other Z-disc proteins [1,2]. The results indicated a

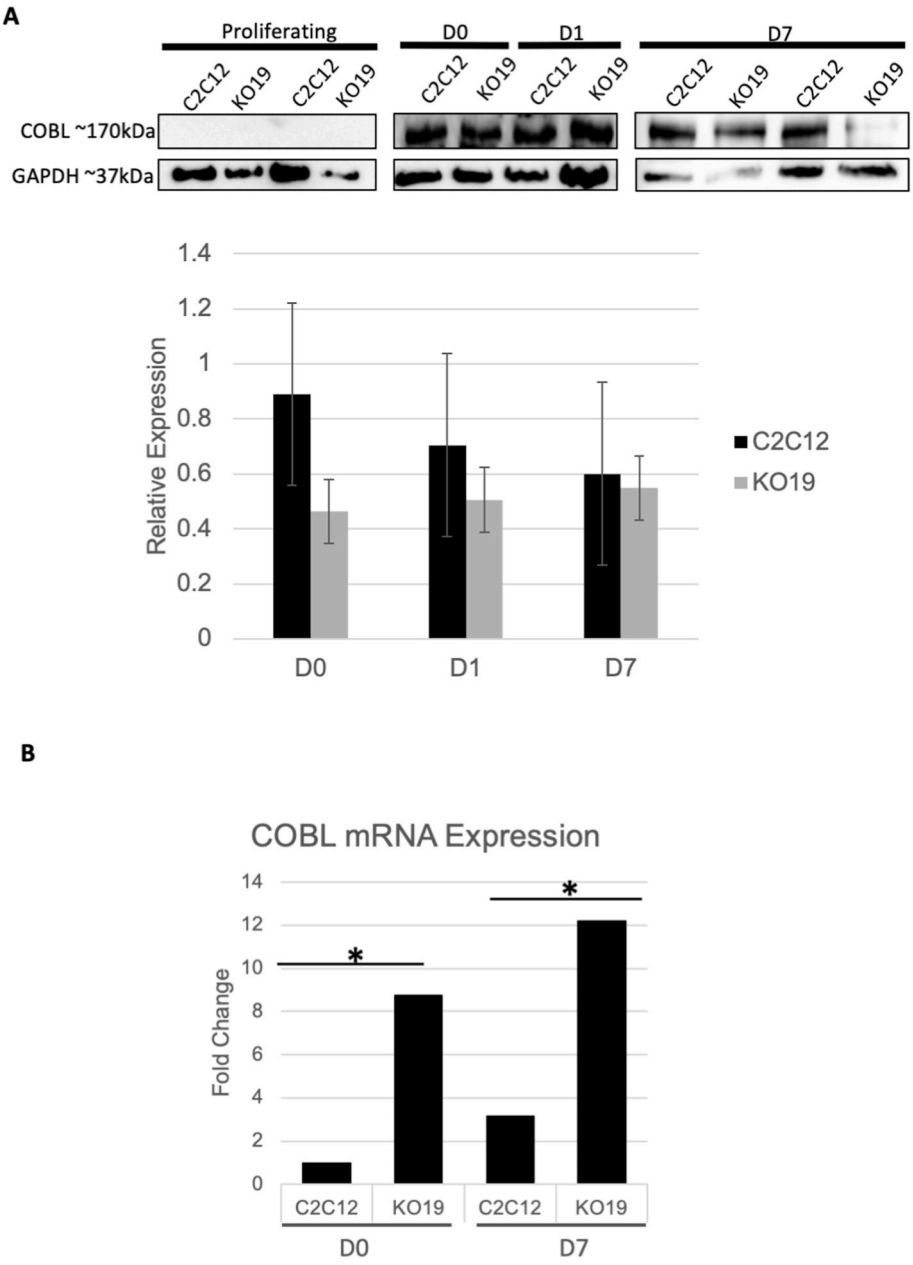

Fig. 5. COBL protein expression throughout in vitro differentiation. A) (Top) Representative Western blots from wildtype C2C12 (C2C12), and IGFN1 knockout (KO19) cells at the following time points: proliferating (P), fully confluent (D0) in differentiation medium for one (D1) or seven (D7) days. Two independent samples are shown for each cell line/timepoint from a total of 4 repeats. (Bottom) Quantification of mean relative COBL expression. Values were normalised to GAPDH expression on a sample by sample basis (n = 4). One-way ANOVA revealed no significant differences between relative expression ($F [7,24] = 0.581$, $p = 0.764$). B) Quantifications of *Cobl* transcript expression. The histograms show the fold change at day 0 (D0) and after 7 days of differentiation (D7). Note that the statistical testing is done on the average *Ct* levels and therefore the standard deviation has not been added to figure. C) C) Cycloheximide treatment of transfected COS7 cells. (Top) Representative Western Blots for COBL-tdTomato in COS7 cells co-transfected with either COBL-tdTomato and GFP, or COBL-tdTomato and IGFN1-GFP (n = 2). Lysates were collected from untransfected control cells (UT) and transfected cells treated with Cycloheximide at 0, 3, 6 and 9 h as indicated. Ponceau red staining of the blots are shown. Black rectangles indicate the portion of the stained blots used for quantification analysis. (Bottom) Densitometry analysis of Western blot bands above, showing averages of relative intensities of COBL-tdTomato to the corresponding densitometry of the lane on the ponceau red.

functional enrichment in the pull-downs of cytoskeletal regulators and proteasome proteins. The actin nucleating COBL protein was selected as a strong candidate. We established that *Cobl* is expressed from the initial phases of C2C12 differentiation when cells align preparing for cell fusion. Although the molecular mechanisms orchestrating vertebrate myoblast fusions are still poorly understood, there is substantial evidence supporting cytoskeletal remodelling as having a fundamental role. Pharmacological inhibition of F-actin polymerization leads to impaired myoblast migration and reduced myoblast fusion [17,18]. During myoblast pairing and alignment, ultrastructural imaging shows the formation of a dense actin wall structure along the length of the plasma membrane of the aligned cells, which regulates cell fusion through vesicle trafficking [19]. Cellular and in vivo models of myoblast fusion have also exposed key regulators of actin remodelling, including the G-protein coupled receptor BAI3 [20] and its intracellular effector DOCK1 [21], the small G-proteins Rac1 and Cdc42 [22], the membrane

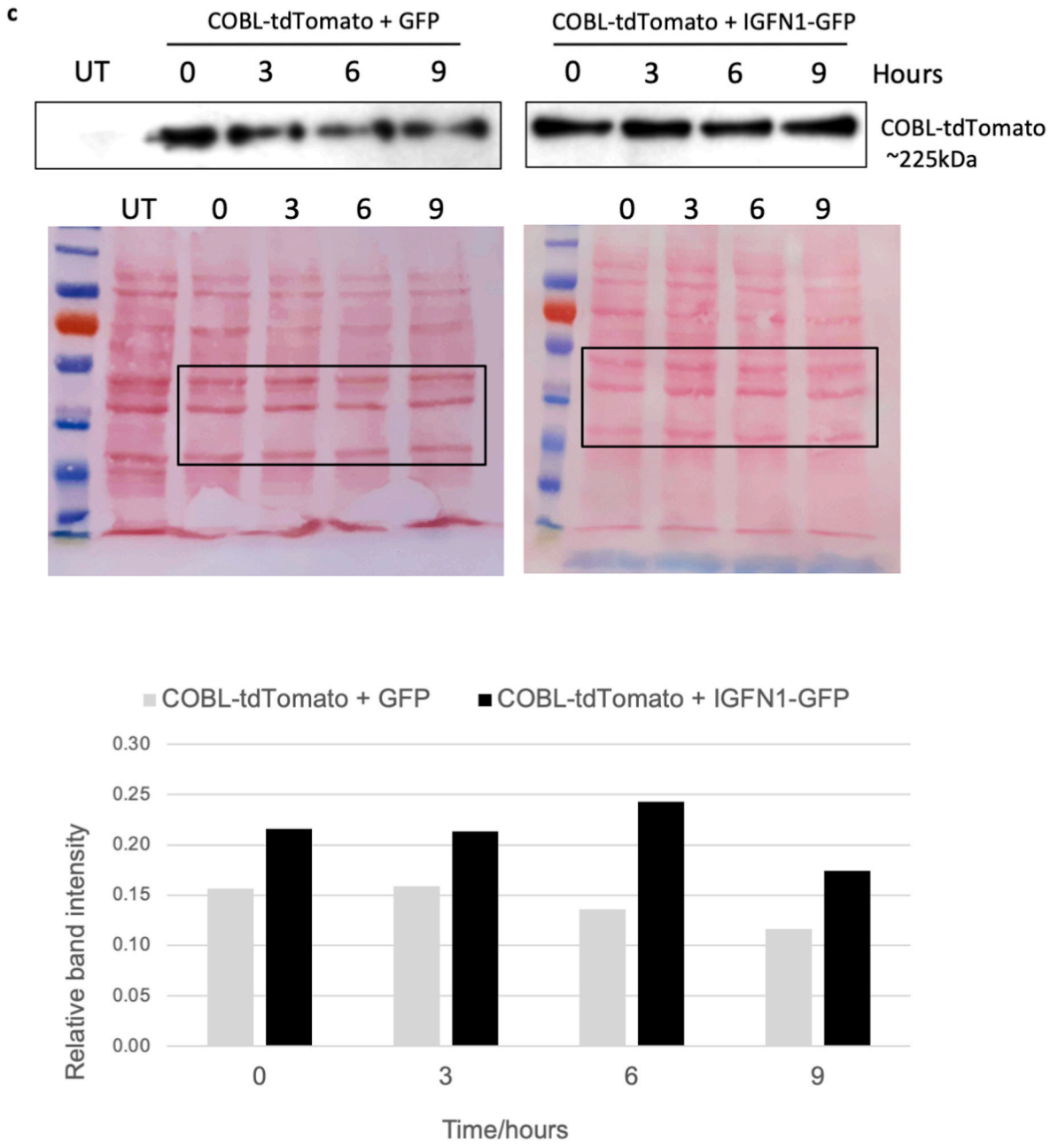

Fig. 5. (*continued*).

and Arp2/3 interacting protein CKIP-1 [23], the adaptor protein and N-WASP binding partner Grb2 [24] and N-WASP itself [25]. Inhibition of F-actin polymerization also impairs the fusogenic activity of the recently discovered fusogens myomaker and minion [26,27]. There is no evidence in the literature of COBL playing a role in fusion or adult muscle. COBL has been shown to be a multifunctional actin regulator, combining G-actin sequestration, weak filament nucleation, powerful filament severing and barbed-end dynamics [28–30]. COBL plays a role in number of specialized processes including neural tube closure [31], neuronal morphology [16], dendritogenesis [32], arborization of Purkinje cells [33], regulation of microvillar length [34], promoting growth of brush border microvilli in the intestine [35] and planar cell polarity [36].

Based on the known functions for COBL and its timing of expression in C2C12 myoblast, we explored a potential role for COBL in myoblast fusion with IGFN1 acting as a scaffold. The interaction between these proteins was first independently validated in the fibroblast COS7. This interaction appears direct, as the cytoplasmic localization of IGFN1 is heavily influenced by the ectopic expression of COBL, resulting in significant protein colocalization in these cells. Moreover, IGFN1 inhibits COBL-mediated ruffle formation in COS7 cells. Such inhibition is not the result of enhanced degradation, as IGNF1 appears to contribute to COBL stability upon cycloheximide exposure. In the more relevant C2C12 cell line, protein COBL levels in *Igfn1* deficient cells also appear lower compared to control cells, despite having significantly higher levels of *Cobl* transcript. Altogether, these results suggest that IGFN1 modulates COBL activity by relocalization or by promoting anti filament building activity of COBL. The functional context of this IGFN1/COBL interaction remains unclear, since C2C12 derived cell lines rendered COBL-deficient by CRISPR/Cas9 mutagenesis were able to fuse at low rates. This is consistent with the recently reported *Cobl* mouse knockout lacking overt muscle defects, though a muscle specific evaluation at morphological or ultrastructural level was not specifically reported [36]. Together, the evidence points at COBL not playing a critical role in myoblast fusion.

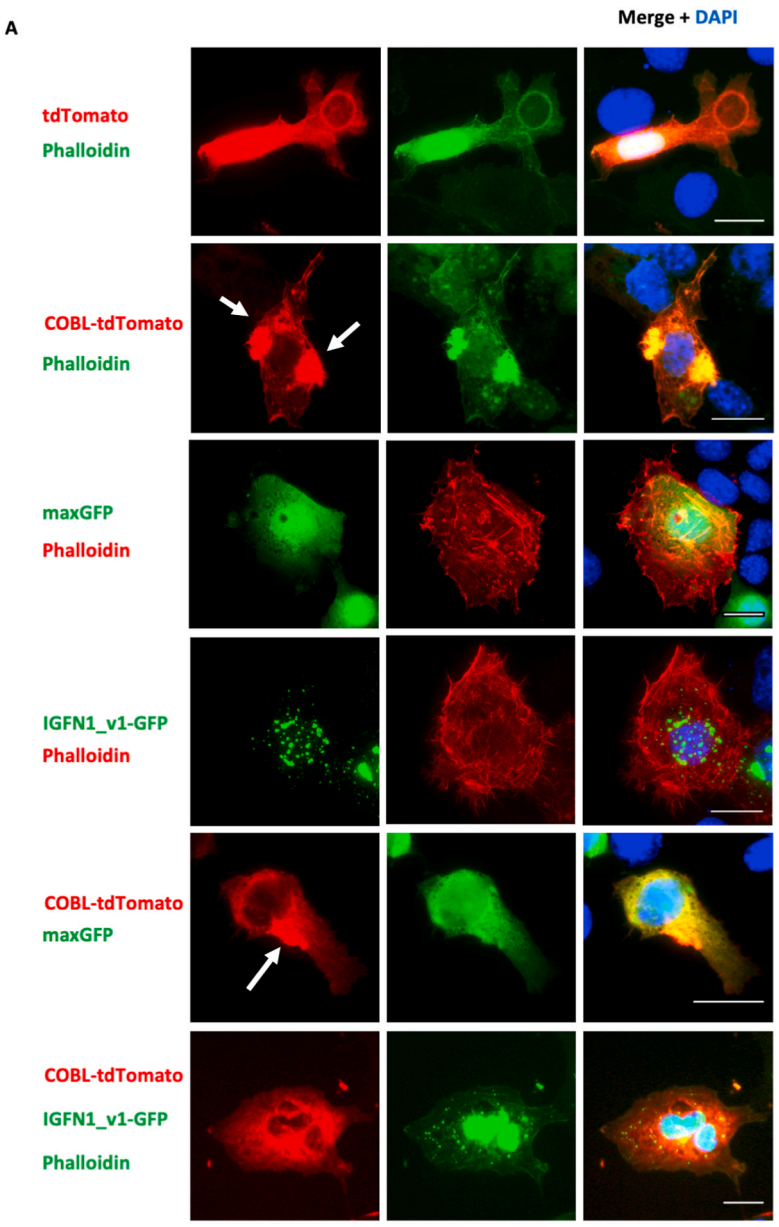

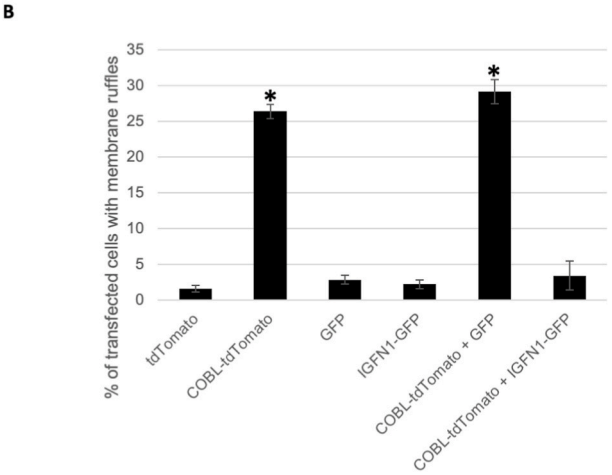

Fig. 6. IGFN1 inhibits COBL-mediated ruffle formation. A) Representative images of transfections of COS7 cells. Transfected constructs are indicated on the left with the font in green or red matching the corresponding fluorescent signal on the images. Phalloidin has been used conjugated to green or red fluorescence as indicated. Ruffles are identified by white arrows. Note that ruffles are detected in cells transfected with COBL-tdtomato alone or co-transfected with maxGFP, but no ruffles are detected in cells co-transfected with COBL-tdtomato and IGFN1_v1-GFP. B) A statistically significant effect of the transfected construct on ruffle percentage was demonstrated by one way ANOVA [$F(5,12) = 117.64$ $p < 0.001$], post-hoc comparisons (Tukey HSD) revealed that ruffle percentage was significantly higher in cells transfected with COBL-tdTomato or COBL-tdTomato + GFP compared with all other conditions except one another ($^*p < 0.01$).

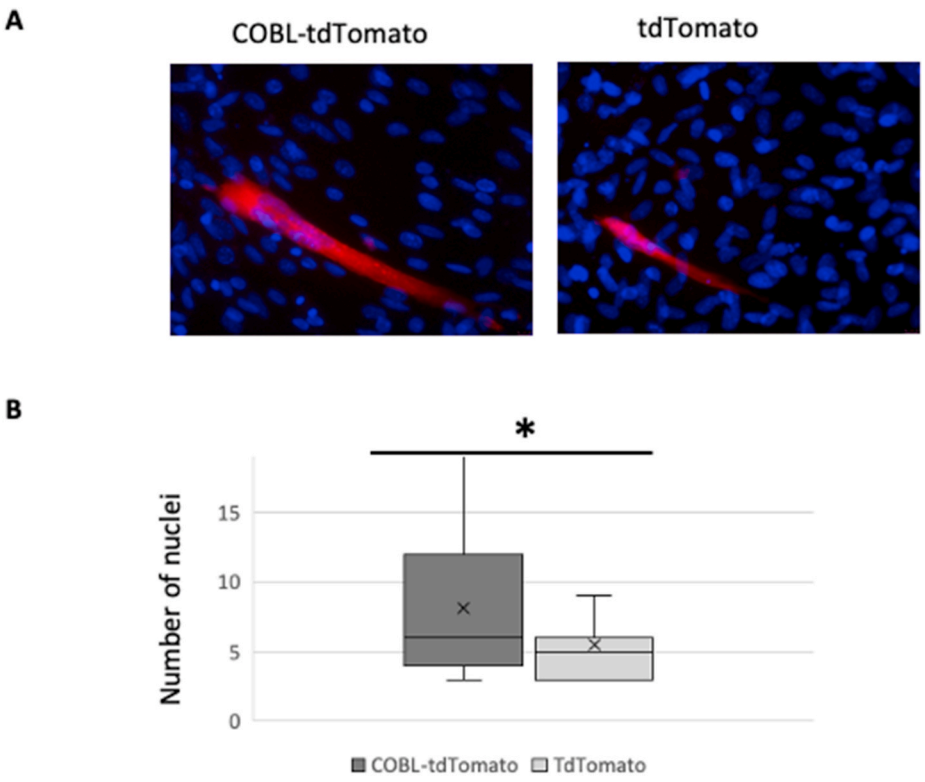

Fig. 7. COBL overexpression increases myoblast fusion. A) Representative images of C2C12 cells transfected with either pDEST47-COBL-tdTomato or pDEST47-tdTomato and differentiated for 7 days. Scale bar represents 50 μm. B) Mean number of nuclei within a pDEST47-COBL-tdTomato or pDEST47-tdTomato expressing myotube (minimum of 3 nuclei to exclude non-fusing cells). The mean number of nuclei was significantly higher in pDEST47-COBL-tdTomato expressing myotubes than in pDEST47-tdTomato expressing myotubes ($n \geq 50$, $p < 0.01$). A minimum of 4 independent transfections were performed per condition.

In the course of these and previous experiments we have concluded that studies looking at fusion and differentiation phenotypes in immortalized myoblasts such as C2C12s are compromised by the effects that clonal selections and subsequent expansions have on the differentiation capacity of the resulting cells. This was attested by the different fusion ability shown by the clonal selection of COBL deficient cell lines, ranging from fusion competent lines (KO18 and KO23) to fusion blunted and no α-actinin expression (KO15). Fusion competent COBL-deficient lines showed a random pattern of α-actinin expression even after long periods of culturing under differentiation conditions. Clonal selection and cell passages may have caused myofibrillogenesis defect in these lines, considering it is a complex process that depends on the orchestrated activity of many proteins [37]. Re-expression of COBL improves α-actinin expression and may suggest a role for COBL in myofibrillogenesis in vitro, but further analyses will be required to determine this.

Localization of COBL to the Z-disc predicts a role for cytoskeleton dynamics in adult muscle. Sarcomeric actin filaments are orientated with their barbed ends (plus ends) anchored at the Z-disc [38]. Since COBL promotes actin assembly at the barbed end [16], it could have a synergistic role of N-WASP, which cooperates with Nebulin to induce actin filament formation in response to a hypertrophic signal at this side of the sarcomere [39]. Interestingly, *Igfn1* expression is downregulated in hypertrophic muscles induced by myostatin inhibition [40], which would free COBL from any IGFN1 inhibitory interaction in these conditions. Conversely, *Igfn1* expression strongly correlates with the induction of muscle loss. Thus, enhancement of myostatin signaling leads to muscle atrophy and dramatic upregulation of *Igfn1* expression [41]. Moreover, *Igfn1* transcripts are induced 100-fold in muscles rendered mechanically inert by denervation [13]. We can therefore speculate that under atrophic conditions, IGFN1 may prevent COBL nucleation activities or stimulate anti filament building abilities of COBL, such as filament severing and G actin sequestration [29].

In summary, our results indicate that COBL is not essential for the focal cytoskeletal remodelling that myoblast fusion relies upon. Further assessment in adult skeletal muscle is required to expose its key role in this tissue.

4. Materials and methods

4.1. In vivo electroporation

C3H/HeJ, 5 ± 8 weeks old, were injected 1 h before the electroporation with 10 μl of 0.4U/μl hyaluronidase (in 0.9% saline). DNA was diluted to 800 ± 1200 ng/μl in ddH2O. 10 μl of DNA samples were loaded into a sterile syringe. Mice were placed in an anesthetizing box with 4% isoflurane in O2 supplied until deeply anaesthetised. Mice were then removed to a heating pad (37C) and continually anaesthetised with a rodent face mask. Toe pinch reflex was used to test the anaesthetic depth. EDL/TA muscles were chosen for these experiments as they are physically confined within the hindlimb and easy to access. Three mm wide electrodes were placed within the muscle and DNA injected between the electrode sites using a preloaded syringe. Pulses were delivered using a NEPA21 machine (Nepagene, Japan) as follows: three 50-msec-long pulses at 100 V followed by three more pulses of the opposite polarity at a rate of one pulse per sec. Mice were sacrificed at 7–30 days after electroporation. EDL/TA muscles were dissected, fixed for 10 min in 4% PFA and snap frozen in liquid nitrogen-cooled isopentane and stored at −80C. Animals were sacrificed by a schedule one killing (cervical dislocation). All animal procedures have been carried with approval from the University of York Ethics committee and followed the UK Animals (Scientific Procedures) Act 1986 Amendment Regulations 2012, performed by under project licence PPL 70/6827 within an approved establishment (licence 5002510).

4.2. Immunohistochemistry

12 μm longitudinal sections of muscle tissue were cut using a cryostat. Sections were permeabilized and blocked using 3% BSA in PBS +0.3% Triton X100 for 1hr. Sections were then incubated overnight at 4 °C with primary antibodies against COBL (Sigma, HPA019167 1:100) or α-actinin (abcam, ab9465 1:100). Slides were then washed in PBST and incubated for 2hrs with appropriate combinations of compatible secondary (either Alexa Fluor 488 goat anti-rabbit or goat anti-mouse,

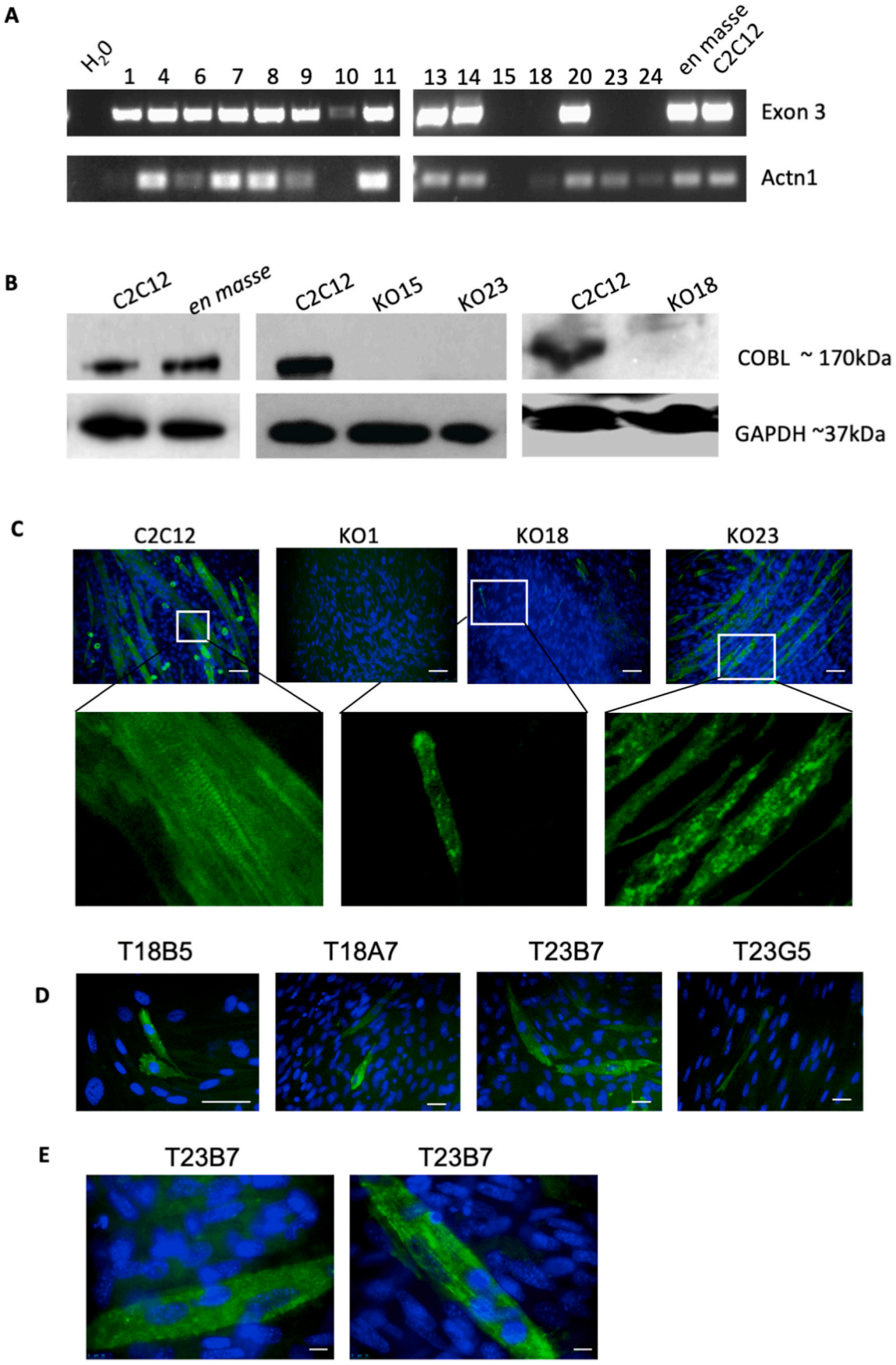

Fig. 8. Generation and characterization of COBL knockout C2C12-derived cell lines. A) Agarose gel showing results from PCR amplifications. Amplicons were obtained with primers flanking exon 3. Amplification of Actn1 to confirm DNA integrity is also shown (Actn1). Amplicons were obtained from 24 individually

selected clones, en masse selection and control C2C12 cells, as indicated. B) Western blot of control C2C12 cells, COBL knockout cells selected en masse and knockout clones KO15, KO18, and KO23. Total loss of COBL is shown for clones KO15, KO18, and KO23. C) Representative images of 7 days differentiated myotubes from control C2C12 cells and COBL knockout clones KO15, KO18 and KO23 stained with anti-α-actinin (green) and DAPI (blue). White squares show amplified insets for C2C12, KO18 and KO23 with no DAPI to show detail. Note α-actinin striations in the control C2C12 cells and α-actinin aggregation pattern in KO18 and KO23. Scale bar represents 75 μm. D) Representative images of 7 days differentiated myotubes from KO18 (T18B5 and T18A7) and KO23 (T23B7 and T23G5) derived cell lines stably expressing pDEST47-COBL-tdTomato and stained with anti-α-actinin (green) and DAPI (blue). Scale bar represents 75 μm. E) Examples from T23B7 taken a 100X. Note the relative improvement of α-actinin expression compared to the parental KO23 cell line shown in C. Scale bar represents 100 μm. F) Plots of differentiation (top) and fusion (bottom) indexes calculated for C2C12, COBL knock-out cell lines (KO18 and KO23) and cell lines stably re-expressing COBL-tdtomato derived from KO18 (T18B5 and T18A7) and KO23 (T23G5 and T23B7). Bars show means and error bars show ±SEM. *Mean differs significantly from C2C12 (Kruskal-Wallis: $P < 0.05$), ** Mean differs significantly from C2C12 (ANOVA: $P < 0.01$).

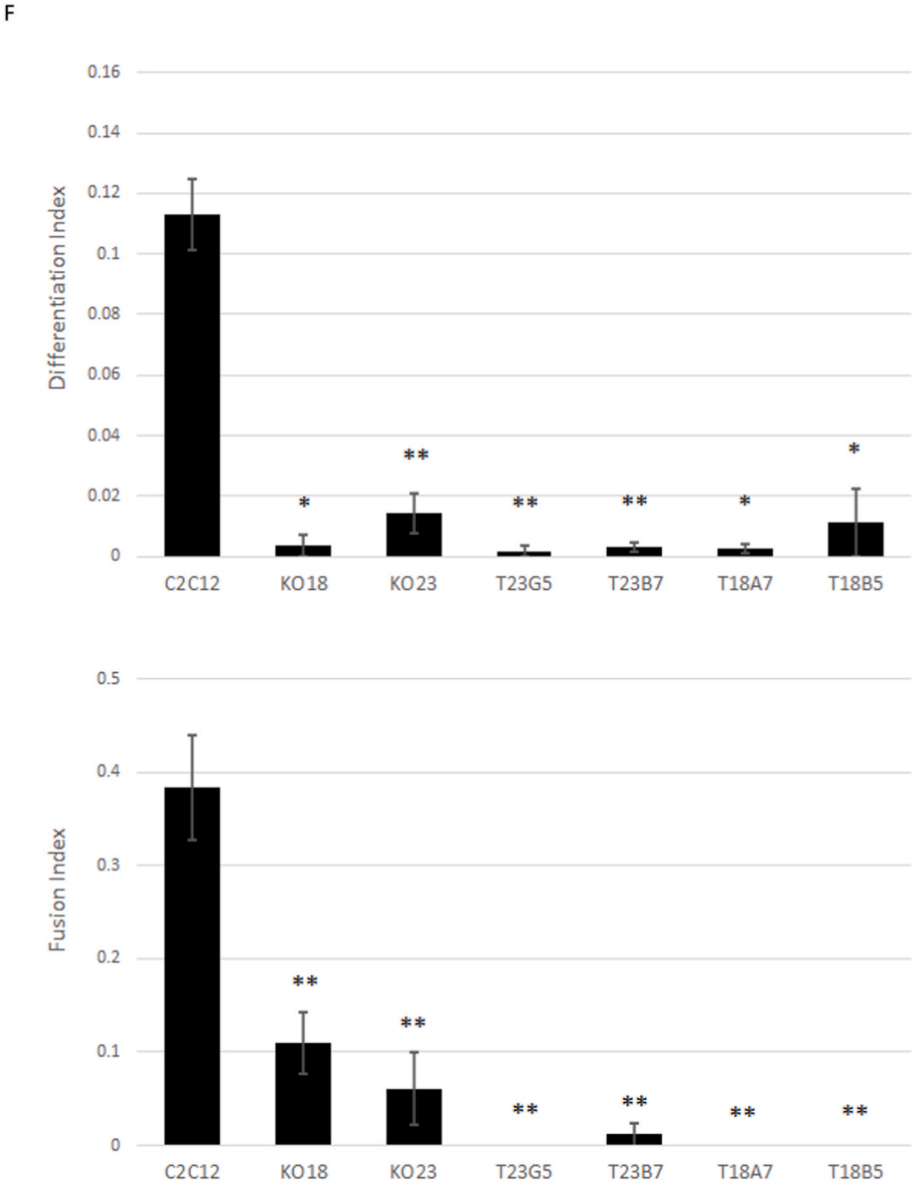

Fig. 8. (*continued*).

Invitrogen R37116/R37120) at RT in the dark before three washes with PBS for 5 min. Slides were mounted with Mowiol plus DAPI to stain nuclei and imaged using a Zeiss Upright 710 confocal microscope.

4.3. Western Blots

For extraction of protein from cells, cells were washed 2 times with PBS on ice, followed by addition of minimal ice-cold RIPA buffer (Sigma, R0278) with protease inhibitors (Sigma, P8340). A cell scraper was used to remove cells from the growth surface and they were then placed on a shaker at 4 °C for 30 min. The sample was then centrifuged (15 min, 12,000 rpm, 4 °C) and the supernatant was transferred to a fresh tube and placed on ice for immediate use or at −80 °C for long term storage. For muscle protein samples, muscle tissue was finely chopped and snap frozen in liquid nitrogen and homogenised in a pestle and mortar. The resulting homogenised tissue was then added into RIPA buffer and incubated at 4 °C for 2 h with shaking. Samples were centrifuged (15 min, 13,000 g, 4 °C) and the resulting supernatant placed in a fresh tube and placed on ice for immediate use or at −80 °C for long term storage.

Typically, 20–50 μg of protein was used per sample along with 4x NuPage LDS buffer (Invitrogen; NP0008) and 10x NuPage sample reducing agent (Invitrogen; NP004). Samples were then heated to 90 °C

for 10 min prior to loading on gels. 10% Bis-Acrylamide Gels were then placed into a bio-rad tank along with running buffer supplemented with NuPage antioxidant (NP0005) and samples loaded. Wet transfers were performed to transfer from gels to nitrocellulose membrane. Gels were placed onto the transfer buffer soaked membrane in between filter paper and fibre pads also soaked in transfer buffer. This was placed in a cassette and loaded into a bio-rad tank and filled with transfer buffer. For 1 h transfers the tank was placed on ice to prevent overheating and run at 100v, for overnight transfers 10v was used. Following transfer, membranes were blocked in 4% skimmed milk powder in PBST (0.01% Tween-20) for 1 h. Primary antibodies (anti-COBL: Sigma, HPA019167 1:300, anti-GAPDH: Sigma, G9295 1:30,000, anti-actin: Cytoskeleton, AAN01 1:250, anti-V5: Sigma, V8137 1:300, anti-His HRP: BIORAD, MCA1396P) were added in blocking buffer and incubated at room temperature for 1 h or overnight at 4 °C. Membranes were then washed in PBST 3 times and HRP-conjugated secondary antibody (anti-rabbit IgG, Santa Cruz Biotechnology, sc-2030 1:10,000) diluted in blocking buffer was added and incubated for 1 h at room temperature. Detection was then performed, following a further 3 PBST washes, using Immobilon Western Chemiluminescent HRP Substrate (Millipore, P09718) in a Chemi-Imager. Densitometry was performed using ImageJ (NIH) to calculate G:F actin ratios, and to measure relative expression of COBL in cell lines, compared to proliferating C2C12 cells, normalised to GAPDH.

4.4. Cloning of COBL

The pENTR Directional TOPO Cloning Kit (Invitrogen, 25–0434) was used to clone COBL into Gateway vectors for mammalian expression. COBL was amplified from a mouse skeletal muscle cDNA library (OriGene Technologies, Inc.) using primers designed to leave blunt-end PCR products with a 5′ CACC to overlap with the GTGG overhang from the pENTR TOPO Vector (forward *caccatggacgcgccgcgtgcactgg*, reverse *cacgagcaagggaacctttcttagt*). Clones were validated by sequencing. LR Clonase II Enzyme Mix (Invitrogen, 11791–020) was used to shuttle the full length COBL cDNA from the entry vector into pDEST47_tdTomato following manufacturer's instructions.

4.5. Cell culture

All cell types were grown in growth medium (GM: DMEM supplemented with 10% FBS and Penicillin Streptomycin (Gibco, 15140122)). For myoblast differentiation cells were grown in GM until they reached 100% confluency whereupon the GM was exchanged for differentiation media (DM: DMEM supplemented with 2% FBS). DM was changed daily. Transfections were performed with the GenJet transfection reagent (SignaGen, Cat # SL100488) using manufacturer's optimised protocols for COS7 or C2C12 cells.

4.6. Ruffle quantification

For single transfections, 20× magnified images were used for quantification. Transfected or total cells in an image were counted using the analyse particles tool in ImageJ. Transfected cells showing membrane ruffles were manually counted and defined as cells displaying a thick band of higher intensity phalloidin at the cell edge. The percentage of cells showing membrane ruffles to the total number of transfected cells was calculated. For co-transfections, 40× magnified images were used for quantifications to distinguish between IGFN1_v1-GFP and green phalloidin. Here, both co-transfected cells and membrane ruffles were manually counted.

4.7. Phalloidin staining and immunostaining of cells

Cells were fixed with 4% paraformaldehyde for 15 min, followed by cell permeabilization with 0.1% Triton X-100 for 5 min and stained with green (CF488 conjugate) or red (594 conjugate) phalloidin for 60 min (1.5 units well-1). Every fixing/staining step was done with two PBS washes. After last PBS wash, coverslips were recovered from wells to dry before a 5 μl Mowiol drop mixed with DAPI (1:1000) was added for mounting coverslips and staining nucleus. For immunostaining, cells were fixed using acetone/methanol for 30 s, followed by overnight incubation in the appropriate antibody (Anti-α-actinin (EA53), abcam ab9465, 1:250 in PBST). Three washes in PBS were performed before incubation in appropriate secondary antibody (AlexaFluor 488 anti-mouse, Invitrogen, R37120), followed by a final three washes and mounting of coverslips using Mowiol with DAPI as above.

4.8. Protein production/purification and pull-down

Protein expression was performed in BL21-AI E. coli (Thermofisher, C607003) expressing either pET161-DEST-Igfn1 (d1-d3) pET161-DEST-Igfn1 (d8-d11). The expression protocol was optimised to maximise soluble protein yield; 100 ml LB was inoculated with overnight starter culture (1:100) and incubated at 37 °C until OD600 = 0.6 where was L-arabinose added (to 0.2% w/v). After 2 h cells were pelleted and fresh LB containing IPTG (1 mM) was added. The culture was incubated overnight at 30 °C with agitation. Protein was purified from bacterial cultures using the ProBond Purification System (Life Technologies, K850-01) under native conditions. Cells were harvested via centrifugation, the resulting pellets were resuspended in 8 ml Native Binding Buffer with lysozyme (1 mg/ml) with protease inhibitors (Sigma, P8849). Cells were then sonicated using six 10 s bursts with at least 10 s on ice between each burst. Lysates were centrifuged at 10,000 g for 15 min to remove cellular debris. 2 ml Ni-NTA agarose beads (Invitrogen, R901-01) were equilibrated in 6 ml Native Binding Buffer before adding the lysate and incubating for 1 h with gentle agitation. Beads were then washed in Native Wash Buffer four times, and the protein left immobilized on the beads and incubated with 1 ml mouse skeletal muscle extract for 1 h with gentle agitation. Beads were then washed in 8 ml Native Wash Buffer four times and 12μL loaded directly onto a 10% Bis/Acrylamide gel and run until the dye front was ~1 cm down the resolving gel. The lane was cut out and sent for LC-MS/MS analysis.

4.9. Immunoprecipitation

For immunoprecipitation, approximately 0.5 mg of protein from cell extracts was first precleared on 25 μl of mouse IgG-Agarose beads (Sigma, A0919) for 1 h at 4 °C on a rotating wheel. This was then centrifuged at 3000 g for 3 min at 4 °C and the resulting supernatant harvested.

A 20μL sample of the supernatant was aliquoted for Western blot analysis as an "input" sample, the rest was divided between either mouse IgG-Agarose beads or Anti-V5 antibody-coupled agarose beads at a concentration of 0.5 mg of protein per 25 μl of slurry and incubated overnight at 4 °C on a rotating wheel. Samples were then centrifuged at 3000 g for 3 min at 4 °C and the supernatant was removed. Bead pellets were then washed four times with 1 ml PBS and pelleted by centrifugation (2mins, 5000 g). After the final wash the beads were prepared for Western blot analysis as described above.

4.10. G/F actin assay

The G-actin/F-actin In Vivo Assay Kit (Cytoskeleton, BK037) was used to isolate G-actin and F-actin fractions following the instructions provided. Briefly, "LAS2 lysis and F-actin stabilization buffer" was added to cells and a cell scraper used to detach cells. Cells were homogenised using a 200 μl pipette tip and incubated at 37 °C for 10 min. This sample was then centrifuged to remove cell debris and the resulting supernatant was removed into an ultracentrifuge tube. The sample was spun at 100,000 g for 1 h at 37 °C, leaving an F-actin pellet and a G-actin supernatant, which was removed. The F-actin pellet was the resuspended in F-actin depolymerisation buffer (using the same volume as the

volume of the initial sample). G-actin and F-actin samples were then analysed via SDS-PAGE western blotting.

4.11. Colocalization analysis

Transfections were performed following manufacturer's instructions (GenJet transfection reagent SL100488, SignaGen, UK). Volocity software (Quorum Technologies) was used for analysis with the Costes method [15] used to set thresholds for calculations of mean Pearson's correlation coefficient. Individual cells were outlined manually in order to select the range of interest selecting only cells expressing both GFP and tdTomato constructs.

4.12. qPCR

All reactions were performed in triplicate giving three technical replicates per biological sample of which a minimum of three were performed. qPCR was performed on the QuantStudio 3 Real-Time PCR System (Applied Biosciences) using the standard fast protocol with melt curve analysis. Data was analysed using the DDCt method measuring target gene expression against a Hprt control. Primers as follows: *cobl* forward *gcctgtcattcaaggccac*, *cobl* reverse *ctgcagtcttccggagcttt*, *Hprt* forward *gttggatacaggccagacttgtt*, *Hprt* reverse *gattcaacttgcgctcatcttagg*, *Myh7* forward *accctcaggtggctccgaga*, *Myh7* reverse *tgcagccccaatgcagcca*.

4.13. Digestion

In-gel tryptic digestion was performed after reduction with dithioerythritol and S-carbamidomethylation with iodoacetamide. Gel pieces were washed two times with aqueous 50% (v:v) acetonitrile containing 25 mM ammonium bicarbonate, then once with acetonitrile and dried in a vacuum concentrator for 20 min. Sequencing-grade, modified porcine trypsin (Promega) was dissolved in 50 mM acetic acid, then diluted 5-fold with 25 mM ammonium bicarbonate to give a final trypsin concentration of 0.02 g/L. Gel pieces were rehydrated by adding 25 L of trypsin solution, and after 10 min enough 25 mM ammonium bicarbonate solution was added to cover the gel pieces. Digests were incubated overnight at 37 °C. Peptides were extracted by washing three times with aqueous 50% (v:v) acetonitrile containing 0.1% (v:v) trifluoroacetic acid, before drying in a vacuum concentrator and reconstituting in 50 L of aqueous 0.1% (v:v) trifluoroacetic acid.

4.14. LC-MS/MS

Samples were loaded onto an UltiMate 3000 RSLCnano HPLC system (Thermo) equipped with a PepMap 100 Å C18, 5 µm trap column (300 µm × 5 mm Thermo) and a PepMap, 2 µm, 100 Å, C18 EasyNano nanocapillary column (75 m × 500 mm, Thermo). The trap wash solvent was aqueous 0.05% (v:v) trifluoroacetic acid and the trapping flow rate was 15 µl/min. The trap was washed for 3 min before switching flow to the capillary column. Separation used gradient elution of two solvents: solvent A, aqueous 1% (v:v) formic acid; solvent B, aqueous 80% (v:v) acetonitrile containing 1% (v:v) formic acid. The flow rate for the capillary column was 300 nL/min and the column temperature was 30 °C. The linear multi-step gradient profile was: 3–10% B over 7 min, 10–35% B over 30 min, 35–99% B over 5 min and then proceeded to wash with 99% solvent B for 4 min. The column was returned to initial conditions and re-equilibrated for 15 min before subsequent injections.

The nanoLC system was interfaced with an Orbitrap Fusion hybrid mass spectrometer (Thermo) with an EasyNano ionisation source (Thermo). Positive ESI-MS and MS2 spectra were acquired using Xcalibur software (version 4.0, Thermo). Instrument source settings were: ion spray voltage, 1900 V; sweep gas, 0 Arb; ion transfer tube temperature; 275 °C. MS1 spectra were acquired in the Orbitrap with: 120,000 resolution, scan range: *m/z* 375–1500; AGC target, 4e5; max fill time, 100 ms. Data dependant acquisition was performed in top speed mode using a fixed 1 s cycle, selecting the most intense precursors with charge states >1. Easy-IC was used for internal calibration. Dynamic exclusion was performed for 50 s post precursor selection and a minimum threshold for fragmentation was set at 5e3. MS2 spectra were acquired in the linear ion trap with: scan rate, turbo; quadrupole isolation, 1.6 *m/z*; activation type, HCD; activation energy: 32%; AGC target, 5e3; first mass, 110 *m/z*; max fill time, 100 ms. Acquisitions were arranged by Xcalibur to inject ions for all available parallelizable time.

Peak lists were converted from. raw to. mgf format using MSConvert (ProteoWizard 3.0.9974) before submitting to a locally-running copy of the Mascot program using Mascot Daemon (version 2.5.1, Matrix Science). Data were searched against the mouse and *E. coli* subsets of the UniProt database (39,956 sequences - Oct 13, 2017) with the following criteria specified: Enzyme, trypsin; Max missed cleavages, 2; Fixed modifications, Carbamidomethyl (C); Variable modifications, Oxidation (M), Deamidated (NQ), Gln- > pyro-Glu (N-term Q), Glu- > pyro-Glu (N-term E), Acetyl (Protein N-term) Peptide tolerance, 3 ppm (# 13C = 1); MS/MS tolerance, 0.5 Da; Instrument, ESI-TRAP. Mascot results in. dat format were imported into Scaffold (version Scaffold_4.8.4, Proteome Software Inc.) and a second database search was performed using the X! Tandem engine with the same criteria specified. Search results were combined in Scaffold and peptide identifications were accepted if they could be established at greater than 86.0% probability to achieve an FDR less than 1.0% by the Scaffold Local FDR algorithm. Protein identifications were filtered to require a minimum of two unique identified peptides. Protein probabilities were assigned by the Protein Prophet algorithm [12]. Proteins that contained similar peptides and could not be differentiated based on MS/MS analysis alone were grouped to satisfy the principles of parsimony. Proteins sharing significant peptide evidence were grouped into clusters.

Complete mass spectrometry data sets are available to download from MassIVE (MSV000083637) and ProteomeXchange (PXD013278). *Pre-publication access can be obtained with the following link ftp://MSV000083637@massive.ucsd.edu, username = MSV000083637, password =* &*RfG87tgˆIKFr.

4.15. Generation of COBL-deficient C2C12 derived clones

Reagents for CRISPR/Cas9 mutagenesis and homologous recombination vectors replacing exons 2, 3 and 4 were obtained from Santa Cruz Biotechnology (sc-419728 and sc-419728-HDR). C2C12 cells were transfected and 24 h later 4 µg/ml puromycin was added for selection. Following 3–4 days of selection, cells selected en masse were processed for PCR analysis and protein extracts. Additionally, clonal selection was undertaken using a serial dilution of puromycin resistant cells in a 96 well plate starting with a stock of ~100 cells/well and seeding at 1:10, 1:50, 1:100, 1:200, and 1:500 across the plate. Wells in which single cells formed a colony were selected for expansion and analysis. Clones (or *en masse* selection) were initially screened by PCR with primers flanking *Cobl* exon 3 (Forward: ATCCTGCCATACCCAATCCT; Reverse: CTTCCCATGCCCACCTCTAG) alongside PCR of α-actinin (Actn1) to control for DNA quality. Selected clones that failed to amplify exon 3 were then tested by Western Blots using anti-COBL antibodies to confirm total absence of COBL protein.

5. Experimental design and statistical rationale

Immunoprecipitations from three samples were analysed with three biological replicates. Samples comprised two regions of IGFN1 and were contrasted with LacZ, which was used as a negative control for non-specific binding. LC-MS/MS sample acquisition was randomised within biological replicate batches – i.e. all samples from biological replicate batch 1 were run before batch 2 but the order of IGFN1(d1-d3), IGFN11(d6-d11) and LacZ within each batch was changed each time. Samples were compared qualitatively using the following criteria. Acceptance of sample group protein identifications as significant to the

pull-down required protein identification probability of greater than 95% in at least two of three biological replicates. Classification of protein absence from the pull-down required protein identification probability of less than 95% in all three biological replicates.

Statistical analysis of data was performed using SPSS (IBM). Data were tested for normality using the Shapiro-Wilk test. Unpaired two-tailed Student's t-tests were used for single comparisons and ANOVA for multiple comparisons with the Tukey HSD multiple comparison test for post-hoc identification of significantly different means.

CRediT authorship contribution statement

Tobias Cracknell: Investigation, Methodology. **Steinar Mannsverk:** Methodology. **Angus Nichols:** Validation, Investigation. **Adam Dowle:** Formal analysis, Methodology. **Gonzalo Blanco:** Supervision, Writing - review & editing, Project administration, Funding acquisition.

Declaration of competing interest

The authors declare no competing or financial interests.

Acknowledgements

We acknowledge the Biology department Technology Facility at the University of York for technical support and the BSF facility for assistance managing the mouse colonies.

Appendix A. Supplementary data

Supplementary data to this article can be found online at https://doi.org/10.1016/j.yexcr.2020.112179.

Funding

T.C was supported by a studentship from the BBSRC White Rose Doctoral Training Programme (BB/M011151/1): Mechanistic Biology and its Strategic Application.

This work was partially funded by a White Rose BBSRC DTP In Vivo Skills Award.

The York Centre of Excellence in Mass Spectrometry was created thanks to a major capital investment through Science City York, supported by Yorkshire Forward with funds from the Northern Way Initiative, and subsequent support from EPSRC (EP/K039660/1; EP/M028127/1).

References

[1] J. Beatham, R. Romero, S.K.M. Townsend, T. Hacker, P.F.M. van der Ven, G. Blanco, Filamin C interacts with the muscular dystrophy KY protein and is abnormally distributed in mouse KY deficient muscle fibres, Hum. Mol. Genet. 13 (2004) 2863–2874.

[2] J. Baker, G. Riley, M.R. Romero, A.R. Haynes, H. Hilton, M. Simon, J. Hancock, H. Tateossian, V.M. Ripoll, G. Blanco, Identification of a Z-band associated protein complex involving KY, FLNC and IGFN1, Exp. Cell Res. 316 (2010) 1856–1870.

[3] G. Blanco, G.R. Coulton, A. Biggin, C. Grainge, J. Moss, M. Barrett, A. Berquin, G. Maréchal, M. Skynner, P. van Mier, et al., The kyphoscoliosis (ky) mouse is deficient in hypertrophic responses and is caused by a mutation in a novel muscle-specific protein, Hum. Mol. Genet. 10 (2001) 9–16.

[4] C. Hedberg-Oldfors, N. Darin, M. Olsson Engman, Z. Orfanos, C. Thomsen, P.F. M. van der Ven, A. Oldfors, A new early-onset neuromuscular disorder associated with kyphoscoliosis peptidase (KY) deficiency, Eur. J. Hum. Genet. 24 (2016) 1771–1777.

[5] R. Straussberg, G. Schottmann, M. Sadeh, E. Gill, F. Seifert, A. Halevy, K. Qassem, J. Rendu, P.F.M. van der Ven, W. Stenzel, et al., Kyphoscoliosis peptidase (KY) mutation causes a novel congenital myopathy with core targetoid defects, Acta Neuropathol. 132 (2016) 475–478.

[6] R. Ebrahimzadeh-Vesal, A. Teymoori, A.M. Dourandish, M. Azimi-Nezhad, Identification of a novel nonsense mutation in kyphoscoliosis peptidase gene in an Iranian patient with myofibrillar myopathy, Genes Dis 5 (2018) 331–334.

[7] E.J. Jokl, G.L. Hughes, T. Cracknell, M.E. Pownall, G. Blanco, Transcriptional upregulation of , a chaperone-assisted selective autophagy factor, in animal models of KY-deficient hereditary myopathy, Dis. Model. Mech. 11 (2018).

[8] J. Beatham, K. Gehmlich, P.F.M. van der Ven, J. Sarparanta, D. Williams, P. Underhill, C. Geier, D.O. Fürst, B. Udd, G. Blanco, Constitutive upregulations of titin-based signalling proteins in KY deficient muscles, Neuromuscul. Disord. 16 (2006) 437–445.

[9] N. Pinotsis, S.D. Chatziefthimiou, F. Berkemeier, F. Beuron, I.M. Mavridis, P. V. Konarev, D.I. Svergun, E. Morris, M. Rief, M. Wilmanns, Superhelical architecture of the myosin filament-linking protein myomesin with unusual elastic properties, PLoS Biol. 10 (2012), e1001261.

[10] C.A. Otey, R. Dixon, C. Stack, S.M. Goicoechea, Cytoplasmic Ig-domain proteins: cytoskeletal regulators with a role in human disease, Cell Motil Cytoskeleton 66 (2009) 618–634.

[11] X. Li, J. Baker, T. Cracknell, A.R. Haynes, G. Blanco, IGFN1_v1 is required for myoblast fusion and differentiation, PloS One 12 (2017), e0180217.

[12] A.I. Nesvizhskii, A. Keller, E. Kolker, R. Aebersold, A statistical model for identifying proteins by tandem mass spectrometry, Anal. Chem. 75 (2003) 4646–4658.

[13] F. Mansilla, C.A.G. Dominguez, J.E. Yeadon, T.J. Corydon, S.J. Burden, C. R. Knudsen, Translation elongation factor eEF1A binds to a novel myosin binding protein-C-like protein, J. Cell. Biochem. 105 (2008) 847–858.

[14] D. Szklarczyk, A. Franceschini, S. Wyder, K. Forslund, D. Heller, J. Huerta-Cepas, M. Simonovic, A. Roth, A. Santos, K.P. Tsafou, et al., STRING v10: protein-protein interaction networks, integrated over the tree of life, Nucleic Acids Res. 43 (2015) D447–D452.

[15] S.V. Costes, D. Daelemans, E.H. Cho, Z. Dobbin, G. Pavlakis, S. Lockett, Automatic and quantitative measurement of protein-protein colocalization in live cells, Biophys. J. 86 (2004) 3993–4003.

[16] R. Ahuja, R. Pinyol, N. Reichenbach, L. Custer, J. Klingensmith, M.M. Kessels, B. Qualmann, Cordon-bleu is an actin nucleation factor and controls neuronal morphology, Cell 131 (2007) 337–350.

[17] J. Dhawan, D.M. Helfman, Modulation of acto-myosin contractility in skeletal muscle myoblasts uncouples growth arrest from differentiation, J. Cell Sci. 117 (2004) 3735–3748.

[18] S.J. Nowak, P.C. Nahirney, A.-K. Hadjantonakis, M.K. Baylies, Nap1-mediated actin remodeling is essential for mammalian myoblast fusion, J. Cell Sci. 122 (2009) 3282–3293.

[19] R. Duan, P.J. Gallagher, Dependence of myoblast fusion on a cortical actin wall and nonmuscle myosin IIA, Dev. Biol. 325 (2009) 374–385.

[20] N. Hamoud, V. Tran, L.-P. Croteau, A. Kania, J.-F. Côté, G-protein coupled receptor Bai3 promotes myoblast fusion in vertebrates, Proc. Natl. Acad. Sci. U.S.A. 111 (2014) 3745–3750.

[21] M. Laurin, N. Fradet, A. Blangy, A. Hall, K. Vuori, J. Cote, The atypical Rac activator Dock180 (Dock1) regulates myoblast fusion in vivo, Proc. Natl. Acad. Sci. Unit. States Am. 105 (2008) 15446–15451. -F.

[22] E. Vasyutina, B. Martarelli, C. Brakebusch, H. Wende, C. Birchmeier, The small G-proteins Rac1 and Cdc42 are essential for myoblast fusion in the mouse, Proc. Natl. Acad. Sci. U.S.A. 106 (2009) 8935–8940.

[23] D. Baas, S. Caussanel-Boude, A. Guiraud, F. Calhabeu, E. Delaune, F. Pilot, E. Chopin, I. Machuca-Gayet, A. Vernay, S. Bertrand, et al., CKIP-1 regulates mammalian and zebrafish myoblast fusion, J. Cell Sci. 125 (2012) 3790–3800.

[24] P. Mitra, T. Thanabalu, Myogenic differentiation depends on the interplay of Grb2 and N-WASP, Biochim. Biophys. Acta Mol. Cell Res. 1864 (2017) 487–497.

[25] Y. Gruenbaum-Cohen, I. Harel, K.-B. Umansky, E. Tzahor, S.B. Snapper, B.-Z. Shilo, E.D. Schejter, The actin regulator N-WASp is required for muscle-cell fusion in mice, Proc. Natl. Acad. Sci. U.S.A. 109 (2012) 11211–11216.

[26] D.P. Millay, J.R. O'Rourke, L.B. Sutherland, S. Bezprozvannaya, J.M. Shelton, R. Bassel-Duby, E.N. Olson, Myomaker is a membrane activator of myoblast fusion and muscle formation, Nature 499 (2013) 301–305.

[27] Q. Zhang, A.A. Vashisht, J. O'Rourke, S.Y. Corbel, R. Moran, A. Romero, L. Miraglia, J. Zhang, E. Durrant, C. Schmedt, et al., The microprotein Minion controls cell fusion and muscle formation, Nat. Commun. 8 (2017) 15664.

[28] C. Husson, L. Renault, D. Didry, D. Pantaloni, M.-F. Carlier, Cordon-Bleu uses WH2 domains as multifunctional dynamizers of actin filament assembly, Mol. Cell. 43 (2011) 464–477.

[29] L. Renault, B. Bugyi, M.-F. Carlier, Spire and Cordon-bleu: multifunctional regulators of actin dynamics, Trends Cell Biol. 18 (2008) 494–504.

[30] Y. Jiao, M. Walker, J. Trinick, J. Pernier, P. Montaville, M.-F. Carlier, Mutagenetic and electron microscopy analysis of actin filament severing by Cordon-Bleu, a WH2 domain protein, Cytoskeleton 71 (2014) 170–183.

[31] E.A. Carroll, D. Gerrelli, S. Gasca, E. Berg, D.R. Beier, A.J. Copp, J. Klingensmith, Cordon-bleu is a conserved gene involved in neural tube formation, Dev. Biol. 262 (2003) 16–31.

[32] L. Schwintzer, N. Koch, R. Ahuja, J. Grimm, M.M. Kessels, B. Qualmann, The functions of the actin nucleator Cobl in cellular morphogenesis critically depend on syndapin I, EMBO J. 30 (2011) 3147–3159.

[33] N. Haag, L. Schwintzer, R. Ahuja, N. Koch, J. Grimm, H. Heuer, B. Qualmann, M. M. Kessels, The actin nucleator Cobl is crucial for Purkinje cell development and works in close conjunction with the F-actin binding protein Abp1, J. Neurosci. 32 (2012) 17842–17856.

[34] J. Wayt, A. Bretscher, Cordon Bleu serves as a platform at the basal region of microvilli, where it regulates microvillar length through its WH2 domains, Mol. Biol. Cell 25 (2014) 2817–2827.

[35] N.E. Grega-Larson, S.W. Crawley, A.L. Erwin, M.J. Tyska, Cordon bleu promotes the assembly of brush border microvilli, Mol. Biol. Cell 26 (2015) 3803–3815.

[36] N. Haag, S. Schüler, S. Nietzsche, C.A. Hübner, N. Strenzke, B. Qualmann, M. M. Kessels, The actin nucleator cobl is critical for centriolar positioning, postnatal

planar cell polarity refinement, and function of the cochlea, Cell Rep. 24 (2018) 2418–2431, e6.
[37] J.W. Sanger, P. Chowrashi, N.C. Shaner, S. Spalthoff, J. Wang, N.L. Freeman, J. M. Sanger, Myofibrillogenesis in skeletal muscle cells, Clin. Orthop. Relat. Res. 403 (2002) S153–S162.
[38] J.W. Sanger, S. Kang, C.C. Siebrands, N. Freeman, A. Du, J. Wang, A.L. Stout, J. M. Sanger, How to build a myofibril, J. Muscle Res. Cell Motil. 26 (2005) 343–354.
[39] K. Takano, H. Watanabe-Takano, S. Suetsugu, S. Kurita, K. Tsujita, S. Kimura, T. Karatsu, T. Takenawa, T. Endo, Nebulin and N-WASP cooperate to cause IGF-1-induced sarcomeric actin filament formation, Science 330 (2010) 1536–1540.
[40] F. Rahimov, O.D. King, L.C. Warsing, R.E. Powell, C.P. Emerson Jr., L.M. Kunkel, K. R. Wagner, Gene expression profiling of skeletal muscles treated with a soluble activin type IIB receptor, Physiol. Genom. 43 (2011) 398–407.
[41] J.L. Chen, K.L. Walton, C.E. Winbanks, K.T. Murphy, R.E. Thomson, Y. Makanji, H. Qian, G.S. Lynch, C.A. Harrison, P. Gregorevic, Elevated expression of activins promotes muscle wasting and cachexia, Faseb. J. 28 (2014) 1711–1723.